# Elucidation of a Structural Basis for the Inhibitor-Driven, p62 (SQSTM1)-Dependent Intracellular Redistribution of cAMP Phosphodiesterase-4A4 (PDE4A4)

Jonathan P. Day,[†] Barbara Lindsay,[‡] Tracy Riddell,[†] Zhong Jiang,[‡] Robert W. Allcock,[‡] Achamma Abraham,[‡] Sebastian Sookup,[†] Frank Christian,[†] Jana Bogum,[§] Elisabeth K. Martin,[‡] Robert L. Rae,[‡] Diana Anthony,[†] Georgina M. Rosair,[‡] Daniel M. Housley,[†] Elaine Huston,[†] George S. Baillie,[†] Enno Klussmann,[§] Miles D. Housley,[†] and David R. Adams[*,‡]

[†]Molecular Pharmacology Group, Division of Biochemistry and Molecular Biology, Institute of Biomedical and Life Sciences, University of Glasgow, Glasgow G12 8QQ, U.K.

[‡]Department of Chemistry, School of Engineering and Physical Sciences, Heriot-Watt University, Riccarton Campus, Edinburgh EH14 4AS, U.K.

[§]Max-Delbrück-Centrum für Molekulare Medizin (MDC), Berlin-Buch, Robert-Rössle-Strasse 10, 13125 Berlin, Germany

Ⓢ *Supporting Information*

ABSTRACT: A survey of PDE4 inhibitors reveals that some compounds trigger intracellular aggregation of PDE4A4 into accretion foci through association with the ubiquitin-binding scaffold protein p62 (SQSTM1). We show that this effect is driven by inhibitor occupancy of the catalytic pocket and stabilization of a "capped state" in which a sequence within the enzyme's upstream conserved region 2 (UCR2) module folds across the catalytic pocket. Only certain inhibitors cause PDE4A4 foci formation, and the structural features responsible for driving the process are defined. Switching to the UCR2-capped state induces conformational transition in the enzyme's regulatory N-terminal portion, facilitating protein association events responsible for reversible aggregate assembly. PDE4-selective inhibitors able to trigger relocalization of PDE4A4 into foci can therefore be expected to exert actions on cells that extend beyond simple inhibition of PDE4 catalytic activity and that may arise from reconfiguring the enzyme's protein association partnerships.
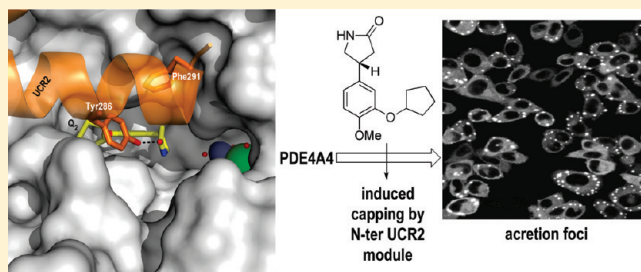
■ INTRODUCTION

Enzymes of the phosphodiesterase type 4 (PDE4) family mediate hydrolytic degradation of cyclic adenosine 3′,5′-monophosphate (cAMP), thereby regulating intracellular concentration gradients of this important second messenger. These enzymes are encoded by four genes (*PDE4A–D*)[1,2] that each give rise to multiple isoforms.[3−7] Cyclic AMP hydrolysis activity is provided by a metallohydrolase core catalytic domain (Figure 1A), which is identical for isoforms arising from any one gene and highly homologous across different gene products. Individual isoforms are distinguished by a unique N-terminal signature sequence that plays a role in targeting the protein to specific signaling complexes and intracellular sites.[2,8−11] The distinct targeting characteristics of PDE4 isoforms are important for controlling the overall spatial integrity of cAMP signaling and orchestrating cross-talk between signaling pathways.[2,12] In this context, it has recently been shown that a fraction of PDE4A4 can be targeted to the plasma membrane in cells expressing the p75 neurotrophin receptor (p75^NTR), a member of the tumor necrosis factor (TNF) receptor superfamily that is up-regulated following

tissue injury.[13,14] The resulting local down-regulation of cAMP suppresses fibrinolysis, and the action of PDE4A4 has consequently been implicated in the pathophysiological processes underlying fibrosis.[13] Inhibition of this particular isoform, or its targeting to p75^NTR, may therefore have useful antifibrotic potential in diseases such as chronic obstructive pulmonary disease (COPD), where PDE4A4 is specifically up-regulated in the lungs of patients[15] and also in spinal cord repair.[16] COPD patients also frequently suffer from sleep deprivation,[17] a condition that, in rodents, causes cognitive deficits through the specific up-regulation of the rodent PDE4A4 orthologue, PDE4A5, in the hippocampus.[18]

We have previously shown that chronic exposure to certain PDE4-selective and competitive inhibitors, such as rolipram, Ro20-1724, and RS-25344, in addition to inhibition of the cAMP hydrolase activity of PDE4A4, also triggers a profound intracellular redistribution of the enzyme into compact accretion foci (Figure 1).[19] This fully reversible process is only associated with
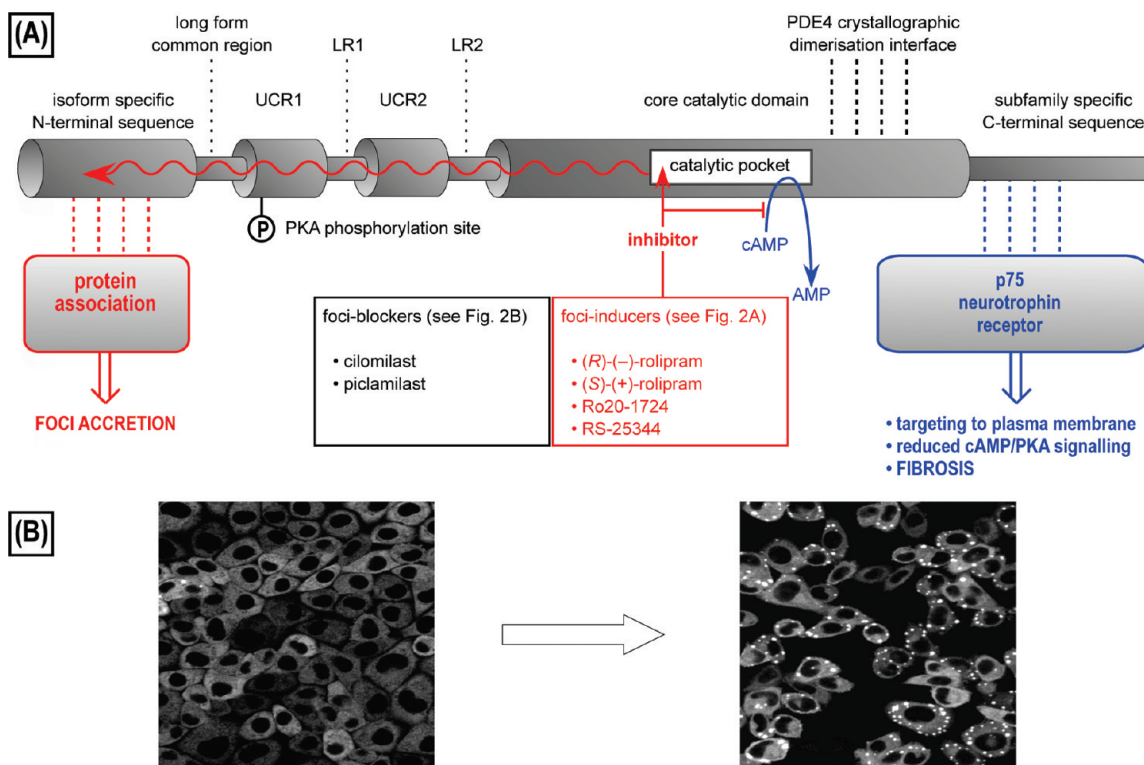
Figure 1. Structural organization of PDE4A4 and model for foci formation. (A) Long PDE isoforms such as PDE4A4 comprise a unique N-terminal sequence connected to a core catalytic domain by two regulatory modules, upstream conserved regions 1 and 2 (UCR1 and UCR2), in series with linker regions (LR1 and LR2). The UCR modules transduce the functional consequences of regulatory phosphorylation by cAMP-dependent protein kinase (PKA). PDE4A4 recruitment to p75[NTR] targets cAMP hydrolase activity to the plasma membrane and has been linked to the pathophysiological suppression of fibrinolysis contributing to fibrosis. Inhibition of PDE4A4 has an antifibrotic action, but in some cases (rolipram, Ro20-1724 and RS-25344) inhibitor occupancy of the catalytic pocket also causes the enzyme's accretion into intracellular foci by inducing or stabilizing protein binding to the N-domain. Other established PDE4 inhibitors (cilomilast and piclamilast) fail to induce foci and antagonize rolipram-induced foci formation. (B) Redistribution of PDE4A4 into accretion foci is most conveniently monitored by confocal microscopy in live CHO cells stably transfected to express a PDE4A4 construct tagged at the C-terminus with green fluorescent protein (GFP). Left, cytoplasmic distribution of PDE4A4-GFP in untreated cells; right, redistribution of PDE4A4-GFP into foci (bright spots) after incubation with (*rac*)-rolipram (3 μM, 10 h).

human PDE4A4 (and the rodent orthologue, PDE4A5) and is not seen with other PDE4 species (including all other known PDE4A isoforms[6,7]), indicating a specific, additional requirement for the unique N-terminal region that characterizes PDE4A4/5. Recently we have further shown that the inhibitor-induced PDE4A4 foci constitute a novel intracellular aggregate state for this enzyme with links to both autophagy and the proteasome system through the association of PDE4A4 with the signaling scaffold and ubiquitin-binding protein p62 (sequestosome-1, SQSTM1).[20] This protein, which is required for the formation of autophagy vesicles,[21] is also associated with ubiquitinated protein aggregates seen in neurodegenerative diseases, such as Lewy bodies in Parkinson's disease, neurofibrillary tangles in Alzheimer's disease, and huntingtin aggregates in Huntington's disease as well as Mallory bodies of alcoholic and non-alcoholic steatohepatitis and hyaline bodies in hepatocellular carcinoma.[22,23]

It is now well-appreciated that the intracellular location of PDE4 species and their recruitment to specific signaling complexes are critical to their functional role in cells not only by underpinning compartmentalized cAMP signaling[2] but, through sequestration of specific proteins, in regulating other signaling pathways, like that of mTor.[24] That certain PDE4 inhibitors can cause the redistribution of PDE4A4, and thereby reconfigure its

partnerships with key proteins linked to fibrosis and autophagy, indicates that such compounds are likely to exert effects that extend beyond those elicited simply by increasing intracellular cAMP levels. An understanding of the SAR surrounding compounds that trigger this action may therefore have an important bearing on the future development of pharmacologically useful PDE4 inhibitors. Our initial studies[19] showed that the effect is driven by inhibitor occupancy of the catalytic pocket but not by elevation of cAMP levels consequent upon inhibition of the enzyme's phosphodiesterase activity. Remarkably, not all PDE4 inhibitors were found to elicit foci formation despite targeting the same catalytic pocket binding site. The structural determinants in an inhibitor responsible for the effect therefore required definition. Here we address this issue, providing insight into the mechanistic basis underpinning the effect.

■ RESULTS AND DISCUSSION

Survey of Established PDE4 Inhibitors for Foci-Forming Activity. We previously showed[19] that both enantiomers of rolipram, Ro20-1724 and RS-25344 induce foci formation with PDE4A4, whereas cilomilast and piclamilast competitively antagonize rolipram-induced foci formation. In order to probe the ligand features responsible for driving the redistribution, we have now
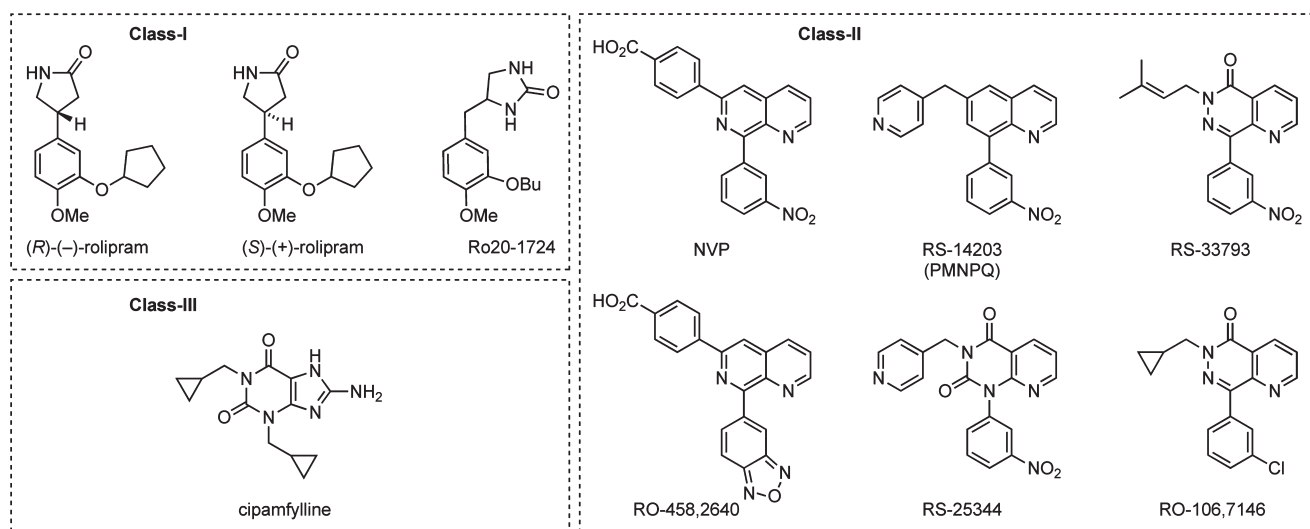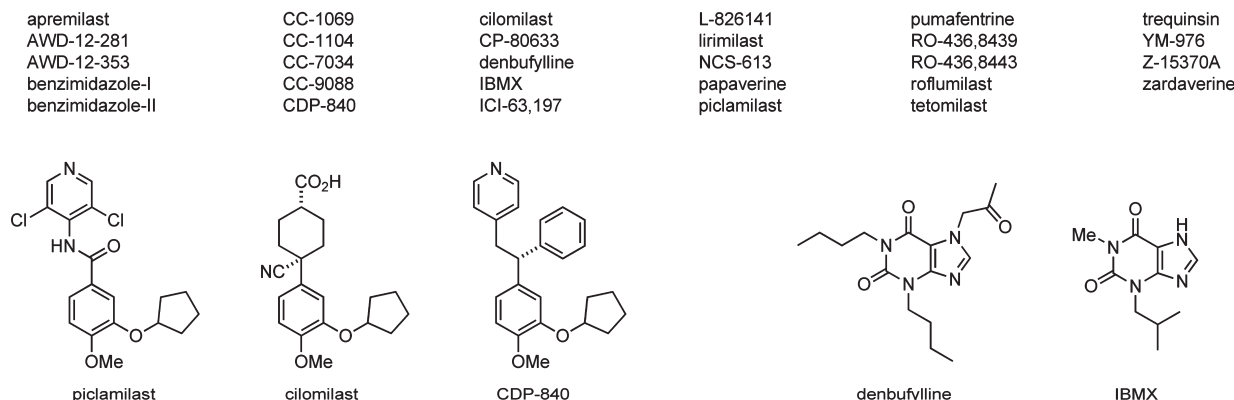
Figure 2. Survey of established PDE4 inhibitors for foci-inducing activity. Compounds were tested according to the procedure described in Terry et al.[19] (A) Structures of PDE4 inhibitors found to induce PDE4A4 foci formation. (B) List of compounds that do not elicit foci formation and that block rolipram-induced foci formation; structures of representative compounds are shown and a full listing by structure is available in the Supporting Information.

undertaken an extensive survey of established PDE4 inhibitors and synthesized novel compounds to gain insight into the mechanistic basis for this action. Most of the existing PDE4 inhibitors evaluated were non-foci-inducing (Figure 2B) and, as might be expected for active-site directed inhibitors, served to block rolipram-induced foci formation. The foci-inducing compounds fell into three distinct structural classes. The catechol ethers, rolipram and Ro20-1724, identified in our earlier study[19] constitute one group (Figure 2A, class I). None of the other 15 catechol ether inhibitors tested (Figure 2B) possessed foci-inducing activity. A second group of foci-inducing compounds (Figure 2A, class II) were all structurally related to RS-25344. Five new compounds were found in this class, namely, NVP, RO-458,2640, RS-14203, RS-33793, and RO-106,7146. These compounds are all based on a 6-substituted 8-arylquinoline template with various combinations of aza and oxo modification in the core quinoline benzo ring. One xanthine-based PDE4 inhibitor, cipamfylline (Figure 2A, class III) was also found to induce foci formation. In contrast, two other established xanthine inhibitors, denbufylline and IBMX (Figure 2B), which are not selective for PDE4 and inhibit various other PDE families, lacked foci-inducing capacity.

Rolipram Lactam Engagement of Metal Centers Is Not Responsible for Foci Formation. The archetypal PDE4-selective inhibitor, rolipram, shares an identical 3-cyclopentyloxy-4-methoxyphenyl core subunit with a number of foci-blocking PDE4-selective inhibitors (piclamilast, cilomilast, and CDP-840). This consideration, reinforced by the observation of a common catechol ether binding mode in the available PDE4 cocrystal structures of rolipram,[25−28] piclamilast,[25] and cilomilast[25] (Figure 3), initially suggested that the determinants for foci induction might reside with the inhibitor auxiliary subunits. These structurally diverse groups, corresponding to the lactam ring in rolipram, are bound proximal to the enzyme's catalytic center, where a more deeply set and tightly bound Zn^{2+} ion (Figure 3 Me1) is paired with a second bivalent metal ion (Me2), which is typically Mg^{2+}.

At the outset of our work, the coordinates of six rolipram-bound PDE4 core catalytic domain cocrystal structures, acquired either with racemic material or with the (R)-antipode, were available in the RCSB Protein Data Bank. In five structures (PDB codes 1OYN, 1OYM, 1TBB, 1XMY, 1XN0)[25,26,28] the rolipram lactam ring (of either enantiomer) makes no direct contact with the metal centers
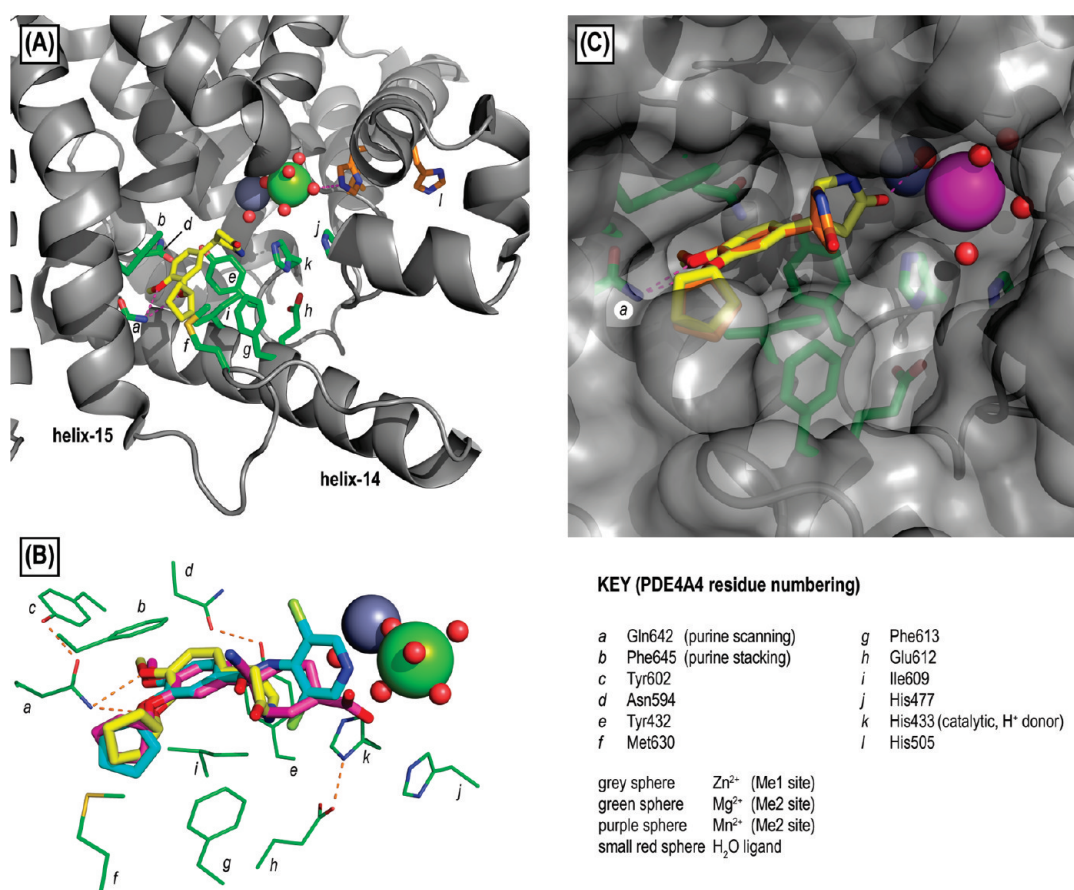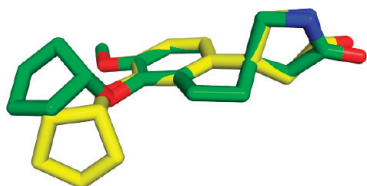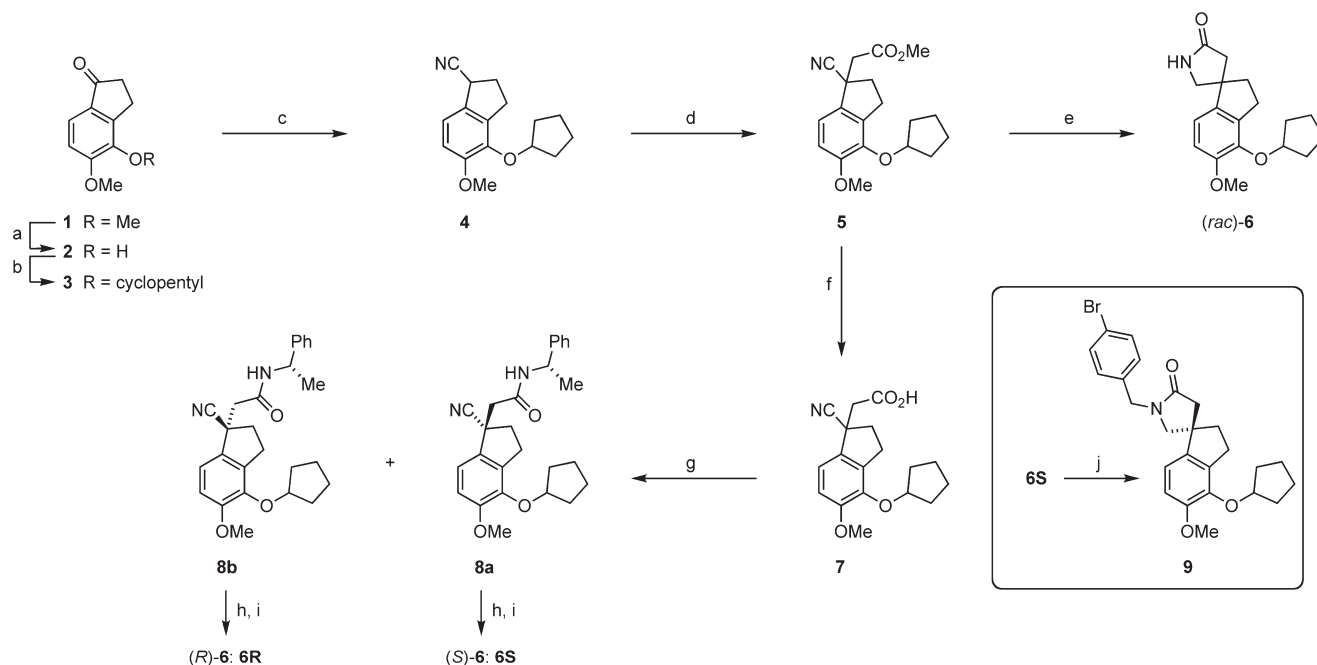
Figure 3. Comparison of rolipram, cilomilast, and piclamilast PDE4-binding modes. (A) PDE4 core catalytic domain with (R)-rolipram (yellow stick, PDB code 1XN0)[25] bound in a solvent-orientated lactam conformation within the catalytic pocket (residues in green stick); mutation of residues highlighted in orange stick has been shown[19] to ablate rolipram-induced foci formation. (B) Overlay of cilomilast (magenta stick) and piclamilast (cyan stick) from their respective PDE4 cocrystal structures (PDB codes 1XLX, 1XM4)[25] onto (R)-rolipram (yellow stick, PDB code 1XN0)[25] showing common binding mode for the core catechol ether subunit. (C) Detail of alternative rolipram binding modes from the 1RO6 PDE4 cocrystal structure:[27] (R)-enantiomer (yellow stick) in metal-orientated mode, (S)-enantiomer (orange stick) in solvent-orientated mode.

but adopts a solvent-orientated conformation with the ring directed toward the opening of the catalytic pocket. In one structure (PDB code 1RO6), acquired with (rac)-rolipram, a mixed population was observed with the inhibitor bound in both the solvent-orientated state and a metal-orientated conformation, the latter with the lactam carbonyl functionality engaging the metal centers and their bridging hydroxide ligand (Figure 3C).[27] Although both enantiomers could be fitted to the electron density for either binding mode, with a slight difference in the axis of the carbonyl group, the electron density for the solvent-orientated binding mode was provisionally attributed to the (S)-enantiomer and that for the metal-orientated mode to the (R)-isomer. In this crystal structure the distance between the Me2 center and the purine-scanning glutamine, the residue that anchors the rolipram catechol ether subunit with hydrogen bonds, is some 3—4% shorter than in the other cocrystal structures with rolipram, piclamilast, and cilomilast. This slightly contracted state allows rolipram to fit between the opposite ends of the pocket, simultaneously engaging the purine-scanning glutamine and the bridging hydroxide at the catalytic center.[29] Thus, the special feature of rolipram as a foci-forming inhibitor might, in principle, be its ability to either induce or stabilize such a contracted state in the cellular environment, perhaps with induced movement in the metal centers providing a basis for the structural transition underpinning foci formation.

We therefore set out to determine whether a metal-orientated enzyme-bound conformation of rolipram is responsible for the compound's foci-inducing capacity. To this end we prepared and evaluated a spirocyclic, torsionally constrained analogue (**6**, Scheme 1) of rolipram. Molecular models suggested that (R)-**6** ought to closely mimic the metal-orientated enzyme-bound conformation of (R)-rolipram in the 1RO6 cocrystal structure. Similarly, (S)-**6** might mimic (S)-rolipram bound in a conformation with the lactam carbonyl orientated toward the enzyme's metal centers. Spirocycle **6** was initially prepared in racemic form according to Scheme 1. Thus, the 4-methoxy group of commercial dimethoxyindanone **1** was selectively demethylated as described by Kemperman et al.[30] Phenol **2** was alkylated with cyclopentyl bromide and the resulting indanone (**3**) converted into nitrile **4** by treatment with p-toluenesulfonylmethyl isocyanide. Alkylation of **4** by treatment with sodium hexamethyldisilazide followed by methyl bromoacetate afforded cyanoester **5**. Synthesis of (rac)-**6** was completed by hydrogenation of the latter at elevated temperature and pressure.

The single crystal X-ray structure of **6** (Figure 4) confirmed that the compound's (R)-enantiomer should be a close structural match for (R)-rolipram bound in the metal-orientated state of the 1RO6 cocrystal structure. However, when tested at concentrations up to 30 μM, spirocycle **6** failed to elicit foci formation in

Scheme 1[a]

[a] Reagents and conditions: (a) Me$_3$N·HCl, AlCl$_3$, CH$_2$Cl$_2$, reflux (93%); (b) bromocyclopentane K$_2$CO$_3$, DMF, 100 °C (85%); (c) TOSMIC, [t]BuOK, MeOH, MeOCH$_2$CH$_2$OMe, 0 °C to room temp (50%); (d) NaHMDS, THF, −78 °C, then BrCH$_2$CO$_2$Me (68%); (e) H$_2$ (16 bar), 10% Pd−C, 60 °C, EtOH, 43 h (66%); (f) LiOH aq, THF, 0 °C (quant); (g) EDC, HOBt, DIPEA, (S)-1-phenylethylamine (1:1 mixture 98%; separated samples of **8a** and **8b** were obtained by HPLC); (h) H$_2$, Raney Ni, EtOH, 90 bar, 90 °C (H-cube); (i) p-xylene, 138 °C, 18 h [two steps, **6S** (75%), **6R** (38%)]; (j) p-bromobenzyl bromide, NaH, DMF (88%).

Figure 4. Single crystal X-ray structure of spirocycle **6** (green stick) shows that the semirigid core of the structure closely superimposes onto the metal-orientated (R)-rolipram conformation (yellow stick) in the 1RO6 crystal structure.

CHO cells expressing PDE4A4-GFP. Moreover, at 30 μM, (rac)-**6** severely inhibited (79 ± 7%; mean ± SD, n = 3) foci induction by (rac)-rolipram (1 μM) and dispersed foci formed by pretreatment of cells with (rac)-rolipram, thus confirming that the compound does compete effectively for the enzyme's catalytic pocket. In order to evaluate the PDE4 inhibitory activity of spirocycle **6** more fully, we prepared the enantiomers for separate assessment by an enantiodivergent extension to the Scheme 1 route. Thus, hydrolysis of ester **5** followed by coupling of the resulting acid (**7**) with (S)-1-phenylethylamine afforded a mixture of diastereomeric amides (**8a/8b**). Chromatographic separation of these compounds followed by hydrogenation of the nitrile and cyclization in hot xylene gave the spirocycle enantiomers (**6R/6S**) for independent evaluation. Unfortunately the intermediate amides (**8a/8b**) did not afford the diffraction quality crystals required for stereochemical elucidation by X-ray crystallography. The absolute configuration of the indanyl stereocenter was therefore determined by subsequent conversion of one of the spirocyclic lactams (**6S**) into its crystalline N-(p-bromobenzyl)

derivative (**9**) and acquisition of a single crystal X-ray diffraction structure (Figure S1, Supporting Information). The separate spirocycle enantiomers (**6R/6S**) both exhibited low micromolar PDE4 inhibitory potency (Table 1) but failed to induce PDE4A4 foci.

N-Alkylated Derivatives of (R)-Rolipram Retain Foci-Inducing Activity. The failure of spirocycle **6** to induce foci suggested that the enzyme-bound state of rolipram responsible for the foci formation may adopt a solvent-orientated lactam conformation. In order to test this proposal, we next evaluated a set of N-alkyl rolipram derivatives, as restricted space in the catalytic pocket proximal to the metal centers (Figure 3C) should sterically preclude the metal-orientated lactam arrangement for such compounds and, effectively, constrain them to a solvent-orientated binding mode. (Bulky structural extensions from the rolipram lactam nitrogen, presumably directed to subsites around the rim of the catalytic pocket, are already known to support or enhance PDE4-inhibitory activity.)[31] Accordingly, we prepared both antipodes of N-methyl and N-benzyl rolipram for assessment (Scheme 2). Significantly, the foci-inducing capacity of (R)-rolipram was retained in both its N-methyl and N-benzyl derivatives (respectively, **10R** and **11R**), supporting the notion that the inhibitor binding with its lactam ring in a solvent-orientated conformation drives foci formation. In contrast, the foci-forming activity of (S)-rolipram was ablated by both N-methylation and benzylation, although derivatives **10S** and **11S** retained activity for inhibition of cAMP hydrolysis by PDE4A4 (Table 1).

The Cyclopentyloxy Group Drives Rolipram-Induced Foci Formation. The failure of **10S** and **11S** to induce accretion foci was surprising because the available cocrystal structures show the lactam N−H bond axis of (S)-rolipram to be orientated directly toward the opening of the catalytic pocket. This suggested that

Table 1. PDE4A4 Inhibitory Activity and Capacity To Induce Foci Formation for Test Compounds[a]

compd	PDE4A4 inhibition		foci induction	
	calcd K_i $(\mu M)^b$	IC$_{50}$ (μM)		EC$_{50}$ (μM)
(rac)-rolipram	0.58	0.83 ± 0.06	yes	0.50 ± 0.08
(R)-(−)-rolipram	0.38	0.55 ± 0.4	yes	0.48 ± 0.09
(S)-(+)-rolipram	3.0	4.3 ± 0.3	yes	3.4 ± 0.9^c
Ro20-1724	3.0	4.3 ± 0.5	yes	3.3 ± 0.2
NVP	0.020	0.029 ± 0.004	yes	0.020 ± 0.008
RS-14203	0.24	0.34 ± 0.02	yes	0.22 ± 0.03
RS-25344	0.015	0.022 ± 0.007	yes	0.017 ± 0.003
RS-33793	0.0077	0.011 ± 0.006	yes	0.015 ± 0.007
RO-458,2640	0.20	0.29 ± 0.05	yes	0.25 ± 0.04
RO-106,7146	0.24	0.34 ± 0.04	yes	0.27 ± 0.03
cipamfylline	1.1	1.6 ± 0.25	yes	0.91 ± 0.3
6S	8.4	12 ± 2	no	n/a
6R	17	24 ± 5	no	n/a
10R	0.7	1.0 ± 0.3	yes	0.5 ± 0.2
10S	1.7	2.4 ± 0.2	no	n/a
11R	2.9	4.3 ± 0.8	yes	2.1 ± 0.9
11S	0.51	0.73 ± 0.09	no	n/a
19R	27	38 ± 8	no	n/a
19S	31	44 ± 14	no	n/a
20R	4.5	6.5 ± 0.6	yes	5.6 ± 0.8
20S	4.5	6.4 ± 0.8	yes	c
21R	4.3	6.2 ± 0.8	yes	4.6 ± 1.9
21S	5.7	8.2 ± 1.5	yes	c
28	3.8	5.4 ± 1.0	no	n/a
ibudilast	0.91	1.3 ± 0.22	yes	0.90 ± 0.1

^{a} Data are given as the mean ± SD for n = 3 independent experiment sets. IC$_{50}$ values with 1 mM cAMP as substrate for PDE4A4 assays. n/a: not applicable. ^{b} K_i values were calculated using the Cheng−Prussof relationship (K_i = IC$_{50}$/(1 + ([cAMP]/K_m))), where the cAMP substrate concentration was 1 mM and the K_m for cAMP hydrolysis by PDE4A4 was 2.3 mM. ^{c} Maximal accretion of PDE4A4 into foci with (S)-enantiomer was maximally <20% of that achieved by the corresponding (R)-enantiomer.

N-alkylation of (S)-rolipram obstructs an induced structural transition that is pivotal for foci formation, perhaps the folding or docking of a protein sequence (e.g., from the enzyme's regulatory N-terminal/UCR regions or a partner protein) across the face of the catalytic pocket. Our previous identification[32] of a protein docking interface for RACK1 on the surface of the PDE4 catalytic unit close to the distal region of the catalytic pocket suggested this idea and caused us to refocus our attention on the role of the rolipram cyclopentyloxy group. This bulky substituent occupies a hydrophobic subpocket (Q$_2$, Figure 5) formed at the junction of orthogonal helices 14 and 15 and their connecting loop (Figure 3A). We considered that the cyclopentyloxy group might stabilize binding of a protein sequence across the catalytic pocket because, like the solvent-orientated lactam, it contributes to the exposed edge of the inhibitor when bound within the catalytic pocket.[33] The cyclopentyloxy group might therefore be essential for foci induction by rolipram. In order to evaluate this, we tested a set of rolipram analogues with smaller alkoxy groups targeted to the Q$_2$ subpocket in place of the cyclopentyloxy. The compounds were prepared (Scheme 3) by an enantiodivergent

Scheme 2^a
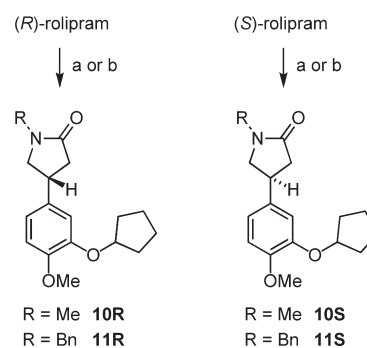
^{a} Reagents and conditions: (a) MeI, NaH, DMF (**10R** 86%, **10S** 63%); (b) BnBr, NaH, DMF (**11R** 76%, **11S** 94%).

strategy similar to that used for synthesis of the spirocycle (**6R/6S**, Scheme 1). A related route was used by Demnitz and colleagues to prepare the parent rolipram enantiomers.[34] Thus, conjugate addition of the nitromethane anion to enone **13** afforded adduct **14**. The latter was converted in three steps into a pair of diastereomeric amides (**17a/17b**) derived from (S)-1-phenylethylamine. Chromatographic separation of these compounds followed by hydrogenation and cyclization of the intermediate aminoamides at elevated temperature afforded the enantiomeric lactams **18R** and **18S**. We had commenced with a benzyloxy group at the 3-position of the precursor arene (**13**) so that the hydrogenation step in the route would also unmask the phenolic function in **18R** and **18S**, allowing convenient parallel alkylation as a final step to deliver the target compound set. In this way we prepared the 3-methoxy, ethoxy, and propyloxy analogues of both rolipram antipodes. The absolute stereochemistry of the two enantiomer series was determined by alkylation of the phenol derived from **17b** with iodocyclopentane; polarimetry identified the product as (S)-(+)-rolipram.

Replacement of the rolipram cyclopentyloxy group by methoxy (compounds **19R/S**) reduced the compound's PDE4-inhibitory activity by an order of magnitude (Table 1). Such activity loss is reasonable given the expected reduction in surface contact between the inhibitor and protein. Significantly, neither enantiomer (**19R/S**) possessed foci-inducing activity at concentrations up to 100 μM. However, both suppressed induction by (rac)-rolipram (1 μM) at these concentrations. Increasing the size of the Q$_2$-targeted substituent from methoxy to ethoxy (**20R/S**) or propyloxy (**21R/S**) unsurprisingly increased the PDE4-inhibitory potency (Table 1), although the compounds were somewhat less effective than the respective parent rolipram enantiomers. Significantly, these compounds were all found to induce accretion foci at concentrations comparable to their PDE4-inhibitory potencies. Thus, substituent occupancy of the Q$_2$ subpocket appears to be a key parameter that controls an inhibitor's capacity to induce foci, with the critical size threshold for foci induction reached with an ethoxy group in the case of the rolipram analogue series.

The Nitrophenyl Group in NVP Drives Foci Formation. During the course of our study, Ke and co-workers disclosed[35] the first PDE4 cocrystal structures of a compound belonging to the class II foci-inducing inhibitors that we have identified. Structures were obtained for NVP in complex with the core catalytic domains from the PDE4A, PDE4B and PDE4D subfamilies (PDB codes 2QYK, 2QYL, and 2QYN). A common

NVP binding mode is seen in these three structures, with the NVP naphthyridine N-1 center anchoring the inhibitor to the purine-scanning Gln and the nitrophenyl group taking the
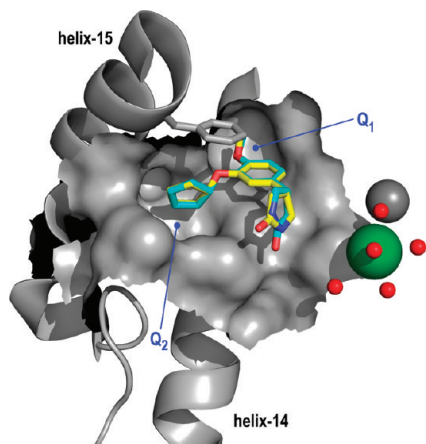

Figure 5. Detail of the PDE4 catalytic pocket taken from the PDE4 cocrystal structure, 1OYN,[26] showing bound (R)-rolipram (yellow stick) and its (S)-enantiomer (cyan stick). The cyclopentyloxy substituent occupies a hydrophobic subpocket formed at the junction of helices 14 and 15 and their connecting loop. Card et al. define this site, adjacent to the purine-scanning Gln, as the Q_2 subpocket.[25] The Q_1 subpocket accommodates the rolipram methoxy group.

position of rolipram's cyclopentyloxy substituent in the Q_2 site (Figure S2, Supporting Information). We thus predicted the nitrophenyl group to be a key foci-driving subunit in NVP and reasoned that an ethyl replacement substituent, which would closely match the 3-methoxy group in **19R/S** for size and bound position, might abolish foci-inducing activity in this representative of the class II group. On this basis, the 8-ethylnapthyridine analogue (**28**) of NVP was prepared for evaluation (Scheme 4).

8-Bromo-1,7-naphthyridin-6-amine (**22**), an intermediate in the synthesis of NVP, was prepared in three steps from pyridine-3-acetonitrile according to the published procedure.[36] Introduction of the ethyl group was achieved by successive Sonogashira coupling of (trimethylsilyl)acetylene, desilylation, and hydrogenation to afford naphthyridinamine **25**. The carboxyphenyl group was then installed following the published route to NVP.[36] Accordingly, diazotization of **25** in the presence trifluoromethanesulfonic acid furnished the triflate (**26**) which was subjected to Suzuki coupling with 4-(methoxycarbonyl)benzeneboronic acid. The resulting ester (**27**) was hydrolyzed under standard conditions to afford target naphthyridine **28**.

Evaluation of **28** in cells expressing PDE4A4-GFP demonstrated, as predicted, that replacement of the NVP nitrophenyl group by the smaller ethyl substituent abolishes the inhibitor's foci-inducing property. However, loss of PDE4-inhibitory potency was also observed with **28** relative to NVP (Table 1). Despite this, **28** clearly retains the capacity to bind in the enzyme's

Scheme 3[a]
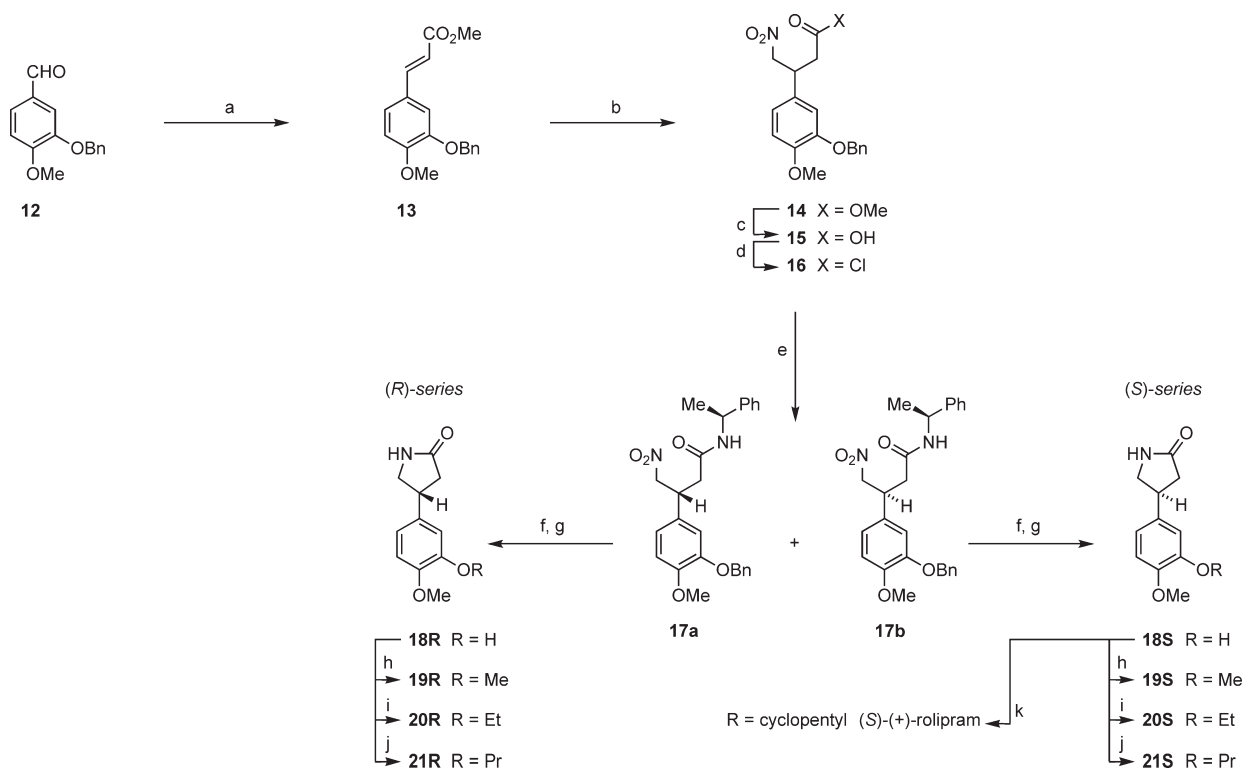
[a] Reagents and conditions: (a) Ph₃P=CHCO₂Me, CH₃CN, reflux; (b) 1,1,3,3-tetramethylguanidine (cat.), MeNO₂, 75 °C (70% two steps); (c) NaOH aq, MeOH, 0 °C (94%); (d) SOCl₂, CH₂Cl₂ (94%); (e) (S)-1-phenylethylamine (1:1 mixture 96%; **17a** and **17b** were then partially separated chromatographically); (f) H₂, 10% Pd−C, EtOH, H₂, EtOAc, EtOH, 90 bar, 90 °C (H-cube); (g) p-xylene, Δ (two steps, **18R** 36%, **18S** 81%); (h) iodomethane, K₂CO₃, DMF (**19R** 87%, **19S** 97%); (i) iodoethane, K₂CO₃, DMF (**20R** 78%, **20S** 96%); (j) 1-iodopropane, K₂CO₃, DMF (**21R** 95%, **21S** 95%); (k) iodocyclopentane, K₂CO₃, DMF, 60 °C (38%).

Scheme 4[a]
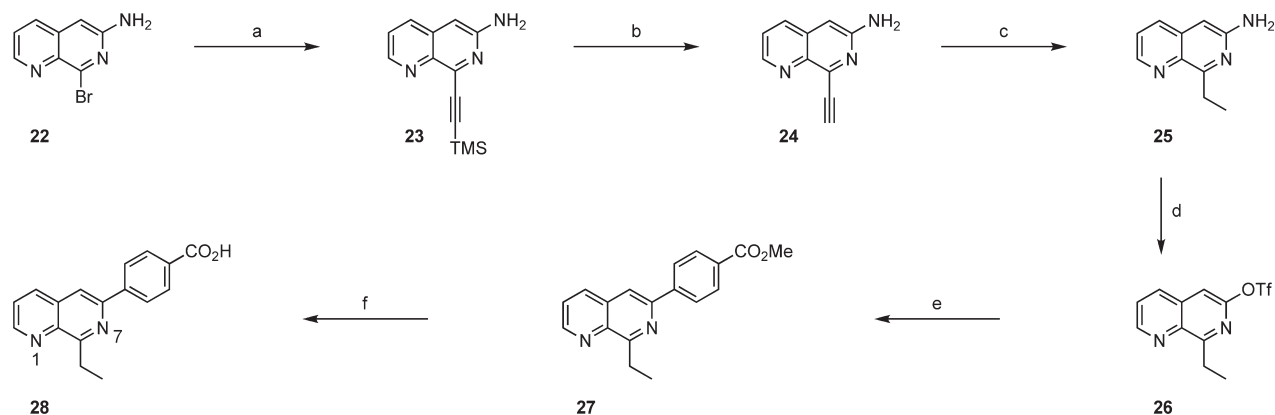
[a] Reagents and conditions: (trimethylsilyl)acetylene, Pd(PPh$_3$)$_2$Cl$_2$, CuI, Et$_3$N, THF, sealed vessel 50–70 °C (30%); (b) TBAF, 95% THF (aq) (85%); (c) H$_2$, Pd/C, EtOH (73%); (d) CF$_3$SO$_3$H, NaNO$_2$, DMF, 0–20 °C (53%); (e) 4-(methoxycarbonyl)benzeneboronic acid, Pd(dba)$_2$, Ph$_3$P, Na$_2$CO$_3$ (aq), THF, reflux (77%); (f) LiOH aq, THF, MeOH (59%).
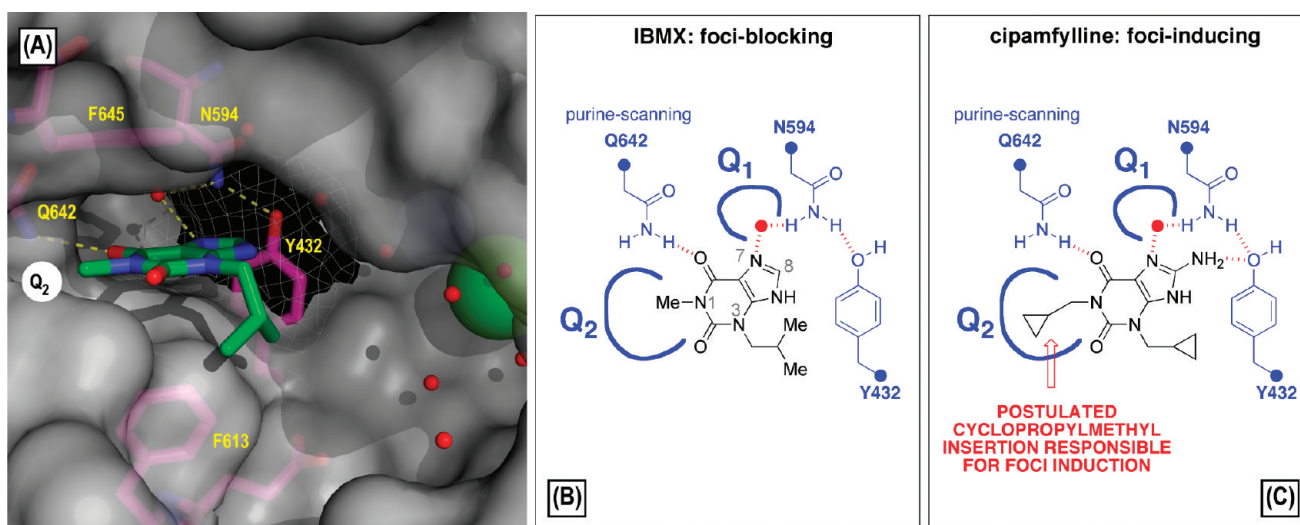

Figure 6. (A) Detail from the IBMX·PDE4 cocrystal structure (PDB code 1ZKN[37]) highlighting key residues in the binding site (PDE4A4 numbering used). (B) Key residue interaction map for bound IBMX (H-bonded water as red circle). (C) Adoption of an IBMX-like binding mode for cipamfylline directs the *N*(1)-(cyclopropylmethyl) group into the Q$_2$ subpocket to drive foci induction. Another binding mode (not shown) in which the cipamfylline 8-NH$_2$ and N-9 center engage Q642 would place the *N*(3)-(cyclopropylmethyl) group into the Q$_2$ subpocket and is a conceivable alternative to that illustrated.

catalytic pocket and, consistent with this, at 10 μM concentration **28** severely inhibited (98 ± 5%; mean ± SD, n = 3) foci induction by (*rac*)-rolipram (1 μM). The other five class II inhibitors of Figure 2A are likely to share a related PDE4 binding mode with NVP, and thus the feature that drives foci formation by these compounds is predicted to be the chlorophenyl group in RO-106,7146, the nitrophenyl unit in the RS series inhibitors, and the benzo[*c*][1,2,5]oxadiazole appendage in RO-458,2640.

The *N*(1)-Cyclopropylmethyl Group of Cipamfylline Is Predicted To Drive Foci Formation. Analysis of the structure of cipamfylline, a foci-forming xanthine inhibitor that is structurally distinct from the class I and class II compounds (Figure 2A), suggests that it too is likely to drive the redistribution of PDE4A4 by insertion of a hydrophobic substituent into the Q$_2$ subpocket. No PDE4 cocrystal structure is available for cipamfylline, but a cocrystal structure has been obtained with the structurally related compound, IBMX,[37] a nonselective PDE inhibitor that does not

trigger foci formation.[19] In this structure the IBMX xanthine core docks into the catalytic pocket with the imidazole ring orientated toward the rear and the 1-methyl group oriented to the front, directed toward the Q$_2$ site (Figure 6A,B). The compound's O^6 center engages the purine-scanning Gln (PDE4A4:Gln642) and a water molecule forms a hydrogen-bonded bridge from N(7) to an asparagine residue in the rear wall of the pocket (PDE4A4: Asn594). Adoption of a similar orientation for cipamfylline (Figure 6C) would be expected to direct a cyclopropylmethyl group into the same Q$_2$ subpocket in which the cyclopentyloxy and nitrophenyl groups of rolipram and NVP act to drive foci induction. The failure of IBMX to show the effect could then be explained by the lack of a sufficiently large substituent targeted to the Q$_2$ subpocket. Denbufylline (Figure 2B), another PDE4-inhibitory xanthine, possesses substituents at N-1 and N-3 (butyl groups) that are comparable in size to the cyclopropylmethyl groups of cipamfylline. In the case of denbufylline, however, the
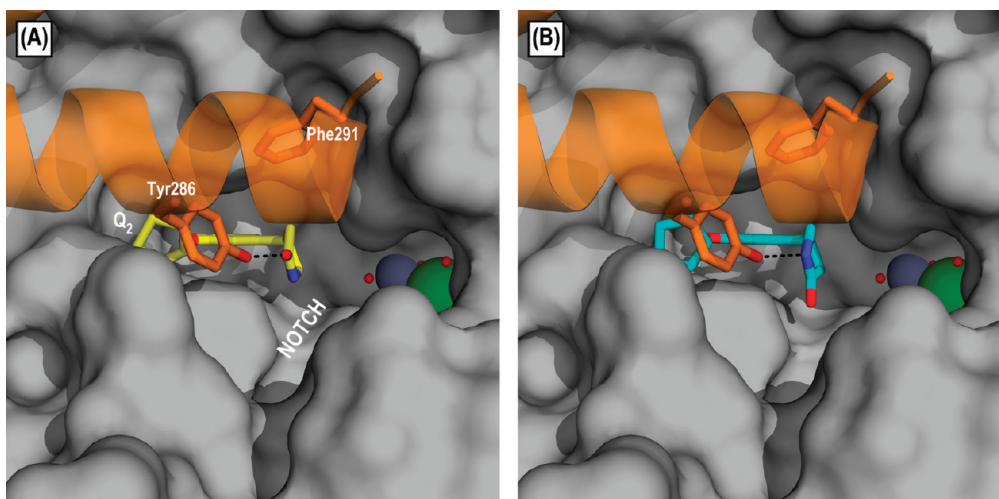
Figure 7. (A) PDE4-bound (*R*)-rolipram (yellow stick, PDB code 1TBB[28]) superimposed into the enzyme's catalytic pocket capped by the UCR2 gating sequence (orange ribbon, PDB code 3G45[38]); lactam *N*-alkyl groups may be accommodated by a notch in the mouth of the catalytic pocket. (B) Similar superimposition to (A) but with (*S*)-rolipram (cyan stick, PDB code 1TBB); lactam N-alkylation is expected to abolish hydrogen bonding to Tyr286 and obstruct capping.

2-oxopropyl substituent at N-7 is likely too bulky for accommodation in the confined Q_1 subpocket within the interior of the cAMP substrate binding cleft. The forced adoption of a binding mode distinct from that observed for IBMX, and postulated here for cipamfylline, may account for the lack of foci-inducing capacity for denbufylline.

Inhibitors Drive Foci Induction through Occupancy of the Q_2 Subpocket and Stabilization of a UCR2-Capped State. The above analysis suggests a unified mechanistic basis for inhibitor-induced PDE4A4 aggregation across the three structurally distinct classes of compound defined in Figure 2A. In each case the process is driven by the targeting of a moderately bulky hydrophobic or aromatic substituent to the enzyme's Q_2 locus in the mouth of the catalytic pocket. Very recently Burgin and co-workers have managed to resolve PDE4 crystal structures that not only contain the PDE4 core catalytic unit but also encompass part of the UCR2 regulatory domain.[38] From this they have postulated that Q_2 subpocket occupancy influences reversible folding of an α-helical motif from the PDE4 regulatory UCR2 module across the opening of the substrate-binding cleft, thereby gating access to the catalytic site.[38] The binding of certain inhibitors within the catalytic pocket may thus serve to stabilize this folding. Significantly, they were able to acquire cocrystal structures for PDE4B and PDE4D in the UCR2-capped state that were stabilized as complexes with RS-14203 and RS-25344, both compounds belonging to the class II foci-inducer group (Figure 2A). UCR2 capping was shown to be critically dependent on the insertion of two aromatic residues from the "UCR2 gating sequence"[39] into the mouth of the catalytic pocket. The cognate residues in PDE4A4 are Tyr286 and Phe291, and the residue corresponding to Tyr286 in particular makes close contact with the Q_2-targeted nitrophenyl group of these inhibitors. In other respects the binding mode of the RS-14203 and RS-25344 core structures closely resembles that observed for NVP (Figure S2, Supporting Information), and the key hydrogen bond from the purine-scanning Gln (to N-1 in NVP) is conserved.

Unfortunately, no crystal structures are currently available for full-length PDE4A4 to provide structural detail for the regulatory UCR1/2 domains and the isoform-specific N-terminal region that is essential for the enzyme's accretion into foci. However, the

recent crystal structures of Burgin et al.[38] support our hypothesis (vide supra) that residues abutting and associated with the catalytic pocket might present a protein docking site. On this basis, we propose a mechanism in which inhibitor-stabilized capping of the catalytic pocket by UCR2 might relay structural transition into the isoform-specific PDE4A4 N-terminal region, thereby inducing or stabilizing the protein—protein associations involved in assembly of accretion foci. To confirm that stabilization of the UCR2-capped state is a key requirement for this process, we mutated Tyr286 and Phe291 independently to Ala and found that both mutations in the UCR2 gating sequence do indeed ablate rolipram-induced foci formation (>97% loss of foci formation compared to WT PDE4A4; $n = 3$ separate experiments).

As recently discussed,[39] the UCR2 capping process in PDE4 may involve a multimeric assembly with the N-termini of paired protein molecules cross-capping the catalytic domains of one another. The importance of dimerization to the function of PDE4 enzymes has excited debate, with controversy still surrounding any possible physiological relevance of the crystallographic dimerization interface (Figure 1A) that is observed almost universally in PDE4 core catalytic domain structures. A key Arg:Asp salt bridge contributes to the crystallographic dimerization interface, and Lee et al. have reported that mutations in this salt bridge compromise dimerization of a PDE4D construct in solution.[40] To probe the relevance of the crystallographically observed core catalytic domain dimer structure to formation of foci, we installed a charge reversal mutation (Arg534Asp) to disrupt the corresponding salt bridge in PDE4A4. Significantly, this mutation also fully ablated induction of foci by rolipram (>96% loss of foci formation compared to WT PDE4A4; $n = 3$ separate experiments), indicating that assembly of PDE4A4 into foci may involve the crossed-UCR2-capped state invoked from recent structural studies.[38,39]

Foci Induction Is Sensitive to the Structure of Inhibitor Auxiliary Subunits. While the presence of a Q_2-targeted hydrophobic substituent of appropriate size is a key parameter that determines the capacity of an inhibitor to drive formation of PDE4A4 accretion foci, the effect is clearly sensitive to the structure of the

inhibitor auxiliary subunit. This sensitivity is strikingly demonstrated in the *N*-alkyl derivatives of rolipram, where alkylation destroys the foci-inducing activity of (*S*)-rolipram but not (*R*)-rolipram (vide supra). A UCR2-capped PDE4 cocrystal structure for rolipram was not obtained by Burgin et al.[38] However, superimposition of bound rolipram from the available crystal structures into the UCR2-capped PDE4B·RS-14203 complex (PDB code 3G45, Figure 7) reveals that the solvent-orientated lactam of both enantiomers is well disposed for hydrogen bonded engagement of the Tyr286 phenolic hydroxyl. For (*R*)-rolipram a close contact from the carbonyl oxygen is expected of the order of 2.5 Å (Figure 7A). In the case of (*S*)-rolipram it is the lactam NH that provides the engagement (Figure 7B), but here the contact is expected to be less tight (O···N distance, ~3.2 Å). This analysis suggests that both the lactam and cyclopentyloxy groups of rolipram contribute to promotion of the UCR2-capped state. The prediction of a weaker hydrogen bond from (*S*)-rolipram to Tyr286 may result in a less pronounced equilibrium shift to the capped state upon binding by this enantiomer compared to (*R*)-rolipram, however, and this may account for our earlier observation[19] that maximal levels of PDE4A4 accretion induced by (*S*)-rolipram are only ~20% of those induced by (*R*)-rolipram, an effect analogous to partial agonism that is uniquely seen for (*S*)-rolipram among the foci-inducing inhibitors that we have identified here.

Inspection of the docked models in Figure 7 also provides a clear rationalization for the impact of N-alkylation on the foci-inducing capacity of the rolipram enantiomers. For (*S*)-rolipram the predicted N−C bond axis of its *N*-alkyl derivatives will be orientated toward Tyr286; N-alkylation will therefore not only abolish the predicted hydrogen bond from the lactam but sterically obstruct capping by the UCR2 gating sequence. In contrast, the corresponding N−C bond axis for *N*-alkyl derivatives of (*R*)-rolipram would be orientated toward a pronounced notch in the rim of the catalytic pocket (Figure 7A) proximal to the metal centers. N-Alkylation of (*R*)-rolipram may therefore be tolerated without disruption of the predicted hydrogen bonded interaction with Tyr286.

Superimposition (not shown) of enzyme-bound structures for cilomilast and piclamilast into the PDE4B·RS-14203 cocrystal structure reveals that these compounds, although sharing a Q$_2$-targeted cyclopentyloxy group, lack a hydrogen bonding feature sufficiently proximal to the side chain of Tyr286 to establish a strong hydrogen bond.[41] This suggests that inhibitor occupancy of the Q$_2$ site with bulky aliphatic groups such as cyclopentyl may alone be insufficient to stabilize the UCR2-capped state and drive formation of foci. In such cases, the docking of Tyr286 appears to require assistance by interaction with additional inhibitor features such as a hydrogen bonding site in the auxiliary subunit, the lactam carbonyl in the case of (*R*)-rolipram and, less optimally, the lactam NH for (*S*)-rolipram. In the case of cipamfylline (Figure 6C) insertion of the cyclopropylmethyl group into the Q$_2$ site would be augmented by a predicted hydrogen bond between the Tyr286 phenol and the inhibitor's 2-O center (O···O distance of ~2.5 Å expected). In contrast the foci-inducing inhibitor, RS-14203 (Figure 2A), clearly lacks additional hydrogen bonding features for engagement of Tyr286. Moreover, this compound's pyridylmethyl extension does not form extensive close contacts directly with the UCR2 gating sequence (PDB code 3G45). This suggests that inhibitors that target the Q$_2$ site with an aryl substituent (nitrophenyl in the case of RS-14203) may not
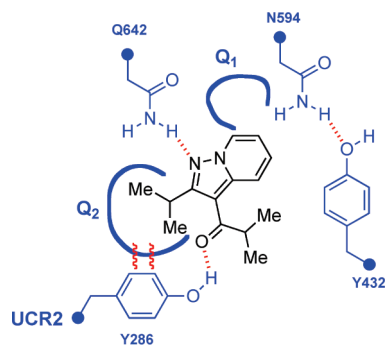
Figure 8. The structure of ibudilast and its predicted PDE4 binding mode are consistent with foci-inducing activity.

require the assistance of a hydrogen bond to Tyr286 in order promote the UCR2-capped state. The targeting of an aromatic inhibitor subunit to the Q$_2$ site may therefore intrinsically stabilize UCR2-capping more effectively, perhaps by establishing efficient π-stacking interactions with Tyr286, than the targeting of an aliphatic group to this location.

These considerations led us to test the impact of a Tyr286Phe mutation on foci induction by rolipram and RS-25344, since our results suggested that loss of a hydrogen bond to Tyr286 should critically compromise the capacity to stabilize UCR2 capping in PDE4A4 (and therefore induction of foci) by the former inhibitor but not the latter. Pleasingly, this analysis was borne out by experiment, and CHO cells expressing Tyr286Phe PDE4A4-GFP exhibited foci when challenged with RS-25344 (94 ± 8% foci formation compared to WT PDE4A4 challenged with RS-25344; mean ± SD, n = 3 separate experiments) but not with rolipram (>97% loss of foci formation compared to WT PDE4A4 challenged with rolipram; n = 3 separate experiments). Our studies imply that effective stabilization of UCR2 capping in PDE4A4 by inhibitors targeting the Q$_2$ site with aliphatic groups such as cyclopentyloxy is very finely balanced and dependent on the establishment of a strong hydrogen bond between the inhibitor auxiliary subunit and Tyr286.

The UCR2 gating sequence is highly conserved across the PDE4 enzyme family,[38] but interestingly PDE4D isoforms are uniquely distinguished by the presence of a phenylalanine at the position corresponding to Tyr286 in PDE4A4. Our results therefore suggest that among the PDE4A, PDE4B, and PDE4D subfamilies, which exhibit widespread tissue distribution, rolipram and related inhibitors should preferentially stabilize UCR2 capping in PDE4A and PDE4B isoforms, whereas inhibitors belonging to the class II foci-inducing group (Figure 2A) may be less discriminating. It is probable, however, that the adoption of a UCR2-capped PDE4 state will be sensitive to the regulatory status of the enzyme, that is, to its specific phosphorylation and protein association status.[39] The impact of inhibitors in modulating UCR2 capping will therefore likely be dependent on context, and extension of our analysis to isoforms beyond PDE4A4 will require investigation in separate studies.

Ibudilast Is Correctly Predicted to Be a Foci-Forming Inhibitor. Having developed an understanding of the inhibitor features responsible for foci induction, we next sought to test this understanding predictively. Ibudilast (Figure 8), a nonselective PDE inhibitor used clinically as an anti-inflammatory agent,[42] was not included in our initial compound screen (Figure 2), which was focused primarily on PDE4-selective inhibitors.

We knew from our experience of developing inhibitors related to ibudilast that pyrazolo[1,5-*a*]pyridines can bind to the PDE4 catalytic pocket with the N(1) center engaging the purine-scanning-Gln.[43] In the case of ibudilast this binding mode would position the 2-isopropyl substituent in the enzyme's Q_2 subpocket with a similar steric demand to the ethoxy and propyloxy groups of the foci-inducing rolipram analogues **20R/S** and **21R/S**. Moreover, in this pose ibudilast's isopropyl ketone would be well-positioned as a hydrogen bond acceptor site to engage Tyr286 in the UCR2 gating sequence (Figure 8), suggesting that the compound should meet the criteria for induction of foci. We therefore tested ibudilast and found that the compound does indeed drive accretion of PDE4A4 into foci (Table 1; 96 ± 7% foci formation compared to PDE4A4 challenged with rolipram; mean ± SD, *n* = 3 separate experiments).

■ CONCLUSION

In summary, evidence for cross-talk between the PDE4 core catalytic and N-terminal domains is well established.[1,2,5−8,11,38,39] Events occurring at regions N-terminal to the catalytic unit, namely, phosphorylation and binding of partner proteins, not only can affect the enzyme's substrate binding and kinetic properties but also can alter sensitivity to inhibition.[39,44−46] Conversely, as in the case of foci formation with PDE4A4, the binding of inhibitors in the catalytic pocket can clearly modulate events that depend on the isoform-specific N-terminus.[19] We show here that the key inhibitor feature driving the intracellular redistribution of PDE4A4 into accretion foci is a moderately bulky hydrophobic or aromatic group targeted to the Q_2 subpocket formed by the junction of catalytic domain helices 14 and 15 and their connecting loop. Reducing the size of this group abolishes foci formation. Our mutagenesis experiments suggest that the Q_2-targeted substituent stabilizes the UCR2-capped state of the enzyme through interaction with Tyr286 in the UCR2 gating sequence, with the resulting structural transition relayed into the N-terminal region. Interactions between Tyr286 and the inhibitor's auxiliary subunit, bound proximal to the enzyme's catalytic metal centers, also play an important role in promoting the UCR2-capped state that leads to foci induction. The presence of an appropriately positioned hydrogen bonding feature that engages the phenolic function of Tyr286 is a characteristic of foci-inducing inhibitors and may be essential for those that possess an aliphatic Q_2-targeted substituent.

There are likely to be over 25 different PDE4 isoforms, each expressed in a cell-type specific fashion and providing specific functional roles in the cells where they are expressed.[8] PDE4A4 is a critical isoform in regulating fibrin deposition through its association with p75[NTR].[13] This has implications for scarring seen in various fibrotic diseases, such as COPD,[14] but also for neuronal growth repair following spinal cord injury,[16] where in each instance the PDE4 inhibitor rolipram has efficacy. The value of PDE4A4 as a potential therapeutic target in COPD is further strengthened by the observation that this isoform is specifically up-regulated in macrophages of COPD patients.[15] Up-regulation of the enzyme in the hippocampus has also recently been shown to underpin cognitive deficits associated with sleep deprivation,[18] a condition prevalent in COPD. Our finding that chronically challenging cells with certain PDE4-selective inhibitors redistributes PDE4A4 into accretion foci through association with p62 but with concomitant loss of partnerships with certain other proteins (such as p75[NTR], DISC1, and *β*-arrestin)[20,47] indicates

that such inhibitors may elicit functional effects not only through PDE4 inhibition but also by disrupting PDE4A4 partnerships and altering subcellular localization. Whether foci formation has positive or confounding actions on therapeutic development has yet to be appreciated and may well depend upon the particular disease target. However, our SAR analysis now provides investigators with a firm structural basis and a library of compounds from different structural classes to assess whether the foci forming attribute of PDE4 inhibitors has positive, deleterious, or null actions on their disease target. This library may additionally provide a toolkit for investigating whether there are endogenous, physiological effectors able to elicit the redistribution of PDE4A4 and thus to dynamically reprogram cAMP compartmentalization by regulating the subcellular targeting of this isoform in the cell. Given the link provided by p62, a scaffold that associates with PDE4A4 and is critical in both foci formation[20] and formation of autophagic vesicles,[21] the compounds described here will also be useful for probing the connection between PDE4A4 foci and autophagy, which may also have bearing on a variety of diseases.

■ EXPERIMENTAL SECTION

Biology. Analyses of inhibitor-driven PDE4A4 foci formation were done as described in detail by us previously.[19,20] PDE4 inhibition was performed as described in detail elsewhere for full-length PDE4A4,[45,48] using a two-step radiochemical assay.[49] Site-directed mutagenesis of plasmid DNA was carried out using the Stratagene (La Jolla, CA, U.S.) QuikChange site-directed mutagenesis kit, according to the manufacturer's instructions. The concentration of DNA samples was determined by spectrophotometrically measuring the absorption at 260 nm (A_{260}). Purified plasmid DNA was produced using the QIAGEN (Crawley, U.K.) QIAprep kits and stored either at 4 °C when eluted in 10 mM Tris-Cl, pH 8.5, or at −20 °C when eluted in sterile water.

Chemistry. Commercially available reagents from Aldrich, Alfa Aesar, and Acros chemical companies were generally used as supplied without further purification. (*R*)-(−)-Rolipram and (*S*)-(+)-rolipram were purchased from Ascent Scientific Ltd. Tetrahydrofuran, diethyl ether, and toluene were dried by distillation from sodium benzophenone ketyl under argon. "Light petroleum" refers to the fraction boiling between 40 and 60 °C. Anhydrous *N,N*-dimethylformamide (DMF) was purchased from Aldrich and used as supplied from Sure/Seal bottles. Reactions were routinely carried out under an inert atmosphere of argon or nitrogen. Analytical thin layer chromatography was carried out using aluminum backed plates coated with Merck Kieselgel 60 GF$_{254}$ (No. 05554). Developed plates were visualized under ultraviolet light (254 nm) and/or alkaline potassium permanganate dip. Flash chromatography was performed using DAVISIL silica (60 Å, 35−70 μm) from Fisher (catalog no. S/0693/60). Fully characterized compounds were chromatographically homogeneous. Melting points were determined using a Stuart Scientific SMP10 apparatus and are uncorrected. IR spectra were recorded on a Perkin-Elmer 1600 FT-IR spectrometer (as KBr discs, as solutions in CHCl$_3$, or as films between NaCl plates) or on a Perkin-Elmer Spectrum 100 FT-IR spectrometer (as neat solids or liquids). Mass spectra were obtained on Kratos Concept IS EI (electron impact) and Fisons VG Quattro (electrospray) spectrometers. ^{1}H NMR spectra were recorded at 200 and 400 MHz on Bruker AC200 and DPX400 spectrometers; ^{13}C NMR spectra were recorded at 50 and 101 MHz on the same instruments. Chemical shifts are recorded in parts per million (δ in ppm) and are referenced against solvent signals (δ_C 77.16 for chloroform and δ_C 39.52 for methyl sulfoxide) for ^{13}C spectra and solvent residual resonances (δ_H 7.26 for chloroform and δ_H 2.50 methyl sulfoxide) for ^{1}H spectra.[50] Chemical shift values are

accurate to ±0.01 ppm and ±0.1 ppm, respectively. *J* values are given in Hz. Multiplicity designations used are as follows: s, d, t, q, sept, and m for singlet, doublet, triplet, quartet, septet, and multiplet, respectively. In ^{13}C NMR spectra, signals corresponding to CH, CH$_2$, or CH$_3$ groups are assigned from DEPT. NMR signal assignments, where reported, were deduced from $^1H-^1H$ COSY, NOESY, HSQC, and HMBC experiments, as appropriate. All compounds tested were >95% pure by elemental and/or HPLC analysis. Elemental analyses were carried out by the analytical service of the Department of Chemistry at Heriot-Watt University using an Exeter CE-440 elemental analyzer.

4-Cyclopentyloxy-5-methoxy-1-indanone (3). A stirred mixture of **2**[30] (12.6 g, 70.7 mmol; prepared as described in the Supporting Information), finely powdered K$_2$CO$_3$ (17.5 g, 126 mmol), and cyclopentyl bromide (10.0 mL, 99.0 mmol) in anhydrous DMF (100 mL) was heated at 100 °C. Further cyclopentyl bromide (4.00 mL, 40.0 mmol) was added after 13 h and a final increment (2.00 mL, 19.8 mmol) together with K$_2$CO$_3$ (8.23 g, 59.5 mmol) after 20 h. Following a total reaction time of 48 h, the mixture was cooled, decanted into brine (1 L), and extracted with Et$_2$O (4 × 100 mL). The combined extracts were dried (Na$_2$SO$_4$) and concentrated in vacuo to a dark brown oil. The title compound (12.4 g, 71%) was isolated as a pale brown solid by crystallization from light petroleum–EtOAc: δ_H (200 MHz, CDCl$_3$) 1.52–1.95 (8H, m), 2.62–2.68 (2H, m), 3.03–3.09 (2H, m), 3.92 (3H, s), 4.89–4.98 (1H, m), 6.95 (1H, d, *J* 8.4), 7.50 (1H, d, *J* 8.4); MS (EI) *m/z* 246 (M$^+$, 9%), 178 (100). Anal. (C$_{15}$H$_{18}$O$_3$) C, H.

4-Cyclopentyloxy-5-methoxy-2,3-dihydro-1H-indene-1-carbonitrile (4). A solution of **3** (2.11 g, 8.59 mmol) in anhydrous DME (20 mL) was added dropwise to a stirred, ice-cooled mixture of *t*-BuOK (3.29 g, 29.3 mmol), TOSMIC (3.10 g, 15.8 mmol), and MeOH (0.988 mL, 24.4 mmol) in anhydrous DME (60 mL) under argon. The mixture was stirred for 30 min at 0 °C and then at ambient temperature for 24 h. The mixture was then partitioned between brine and EtOAc and the organic layer dried (Na$_2$SO$_4$) and concentrated in vacuo. The resulting crude product was subjected to flash column chromatography (9:1 light petroleum–EtOAc) to afford **4** (1.11 g, 50%) as a yellow solid: δ_H (400 MHz; CDCl$_3$) 1.54–1.64 (2H, m), 1.64–1.76 (2H, m), 1.78–1.88 (4H, m), 2.34 (1H, dq, *J* 12.8 and 8.1), 2.52 (1H, dtd, *J* 12.6, 8.0 and 4.4), 2.88 (1H, dt, *J* 16.1 and 8.0), 3.08 (1H, ddd, *J* 16.2, 8.6 and 4.4), 3.83 (3H, s), 4.05 (1H, t, *J* 8.0), 4.83–4.87 (1H, m), 6.81 (1H, d, *J* 8.2), 7.06 (1H, d, *J* 8.3); MS (EI) *m/z* 257 (M$^+$, 51%). Anal. (C$_{16}$H$_{19}$NO$_2$) C, H, N.

Methyl 2-(1-Cyano-4-cyclopentyloxy-5-methoxy-2,3-dihydro-1H-inden-1-yl)ethanoate (5). NaN(SiMe$_3$)$_2$ (1.0 M THF solution, 22.0 mL, 22.0 mmol) was added dropwise to a solution of **4** (4.50 g, 17.5 mmol) in anhydrous THF (200 mL) at −78 °C. The mixture was maintained at −78 °C for 5 h, brought to 10 °C for 1 h, and then returned to −78 °C before adding methyl bromoacetate (3.60 mL, 38.0 mmol). The mixture was then allowed to attain ambient temperature and, after a further 16 h, partitioned between EtOAc (500 mL) and brine (200 mL). The organic phase was dried (Na$_2$SO$_4$) and concentrated in vacuo to yield the crude product, which was subjected to flash column chromatography (1:4 to 7:13 Et$_2$O–hexane gradient elution) and crystallization (Et$_2$O–hexane–CH$_2$Cl$_2$) to afford **5** (3.92 g, 68%) as a colorless solid: δ_H (400 MHz, CDCl$_3$) 1.53–1.64 (2H, m), 1.64–1.76 (2H, m), 1.77–1.88 (4H, m), 2.37 (1H, ddd, *J* 13.3, 7.8 and 5.6), 2.69 (1H, d, *J* 16.0), 2.72 (1H, ddd, *J* 13.3, 8.4, and 6.5), 2.98 (1H, d, *J* 16.0), 2.91–3.09 (2H, m) 3.74 (3H, s), 3.83 (3H, s), 4.81–4.90 (1H, m), 6.81 (1H, d, *J* 8.7), 7.04 (1H, d, *J* 8.3); MS (EI) *m/z* 329 (M$^+$, 42%). HRMS (EI) calcd for M$^+$ C$_{19}$H$_{23}$NO$_4$ 329.1627, found 329.1615. Anal. (C$_{19}$H$_{23}$NO$_4$) C, H, N.

(rac)-4-Cyclopentyloxy-5-methoxy-2,3-dihydrospiro[indene-1,3'-pyrrolidin]-5'-one (6). A solution of **5** (97.0 mg, 0.295 mmol) in a mixture of absolute EtOH (5 mL) and EtOAc (5 mL) containing AcOH (2 drops) was hydrogenated over 10% Pd–C (10.0 mg) at 60 °C and 16 bar of H$_2$ pressure for 43 h. The mixture was then purged with N$_2$ and filtered

over Celite, washing with EtOAc. The filtrate was concentrated in vacuo and the crude product subjected to flash column chromatography (EtOAc) followed by crystallization (CH$_2$Cl$_2$–Et$_2$O) to afford **6** (58.6 mg, 66%) as a colorless solid: NMR data, as presented for **6S**; MS (EI) *m/z* 301 (M$^+$, 49%. HRMS (EI) calcd for M$^+$ C$_{18}$H$_{23}$NO$_3$ 301.1678, found 301.1673. The structure was confirmed by single crystal X-ray diffraction (Supporting Information).

2-(1-Cyano-4-cyclopentyloxy-5-methoxy-2,3-dihydro-1H-inden-1-yl)ethanoic Acid (7). Ester **5** (2.99 g, 9.07 mmol) was hydrolyzed with LiOH·H$_2$O (577 mg, 13.8 mmol) in a vigorously stirred mixture of THF (35 mL) and water (17 mL) at 0 °C for 1 h and then at ambient temperature for 3 h. The mixture was concentrated in vacuo to afford a white slurry that was taken up in water (500 mL). NaOH solution (2 M, 10 mL) was added and the basic solution washed with Et$_2$O (100 mL). The organic extract was discarded; the aqueous phase was then acidified to pH 1 with concentrated hydrochloric acid and extracted with CHCl$_3$ (3 × 100 mL). The combined extract was dried (Na$_2$SO$_4$) and evaporated to afford acid **7** (2.90 g, quant) as a white amorphous solid: δ_H (200 MHz, CDCl$_3$) 1.52–1.91 (8H, m), 2.37 (1H, ddd, *J* 13.3, 7.4, and 6.0), 2.69–3.16 (3H, m), 2.76 (1H, d, *J* 17.6), 3.06 (1H, d, *J* 17.6), 3.84 (3H, s), 4.82–4.90 (1H, m), 6.83 (1H, d, *J* 8.4), 7.07 (1H, d, *J* 8.3).

2-[(S)-1-Cyano-4-cyclopentyloxy-5-methoxy-2,3-dihydro-1H-inden-1-yl]-N-[(S)-1-phenylethyl]ethanamide (8a) and 2-[(R)-1-Cyano-4-cyclopentyloxy-5-methoxy-2,3-dihydro-1H-inden-1-yl]-N-[(S)-1-phenylethyl]ethanamide (8b). To a stirred solution of **7** (2.86 g, 9.07 mmol) and 1-hydroxybenzotrazole (1.53 g, 9.96 mmol) in anhydrous DMF (30 mL) at 0 °C was added 1-ethyl-3-(3'-dimethylaminopropyl)carbodiimide hydrochloride (2.11 g, 11.0 mmol) followed by N,N-diisopropylethylamine 1.60 mL, 10.3 mmol). After 30 min (S)-1-phenylethylamine (1.65 mL, 12.0 mmol) was added. The mixture was stirred at 0 °C for 3 h and then at ambient temperature for 24 h. Et$_2$O (300 mL) and EtOAc (75 mL) were added, and the mixture was washed successively with brine (100 mL), hydrochloric acid (1 M, 3 × 100 mL), saturated NaHCO$_3$ solution (2 × 100 mL), and brine (100 mL). The organic phase was dried (Na$_2$SO$_4$) and evaporated. The resulting residue was subjected to flash column chromatography to afford the product (3.73 g, 98%), a 1:1 mixture of **8a** and **8b**, as a colorless powder. Separated samples of **8a** (500 mg, 99.5% purity) and **8b** (402 mg, 98% purity) were obtained by HPLC. Isomer **8a**: HPLC t_R = 9.21 min (160 mm × 4.5 mm Thermo Scientific Hypersil 5 μm silica column; 2:12:86 MeOH–CH$_2$Cl$_2$–hexane mobile phase at 1 mL/min); δ_H (400 MHz, CDCl$_3$) 1.50 (3H, d, *J* 6.9), 1.54–1.64 (2H, m), 1.64–1.75 (2H, m), 1.77–1.88 (4H, m), 2.53 (1H, d, *J* 14.1), 2.54 (1H, ddd, *J* 13.3, 7.9, and 5.7), 2.63 (1H, ddd, *J* 13.3, 8.3, and 6.6), 2.75 (1H, d, *J* 14.1), 2.93 (1H, app dt, *J* 16.4 and 7.3), 3.02 (1H, ddd, *J* 16.4, 8.3, and 5.8), 3.82 (3H, s), 4.82–4.86 (1H, m), 5.12 (1H, quintet, *J* 7.2), 5.90 (1H, br d, *J* 7.8), 6.77 (1H, d, *J* 8.3), 6.96 (1H, d, *J* 8.3), 7.24–7.35 (5H, m). Isomer **8b**: HPLC t_R = 9.74 min (160 mm × 4.5 mm Thermo Scientific Hypersil 5 μm silica column; 2:12:86 MeOH–CH$_2$Cl$_2$–hexane mobile phase at 1 mL/min); δ_H (400 MHz, CDCl$_3$) 1.43 (3H, d, *J* 6.9), 1.54–1.64 (2H, m), 1.64–1.75 (2H, m), 1.77–1.88 (4H, m), 2.47 (1H, ddd, *J* 13.3, 7.8, and 5.6), 2.57 (1H, d, *J* 14.2), 2.59 (1H, ddd, *J* 13.3, 8.4, and 6.7), 2.75 (1H, d, *J* 14.2), 2.94 (1H, app dt, *J* 16.4 and 7.9), 3.02 (1H, ddd, *J* 16.4, 8.6, and 5.8), 3.82 (3H, s), 4.83–4.89 (1H, m), 5.09 (1H, quintet, *J* 7.2), 5.83 (1H, br d, *J* 7.7), 6.76 (1H, d, *J* 8.3), 6.99 (1H, d, *J* 8.3), 7.23–7.35 (5H, m). Anal. (1:1 **8a**/**8b** mixture, C$_{26}$H$_{30}$N$_2$O$_3$) C, H, N.

(S)-4-Cyclopentyloxy-5-methoxy-2,3-dihydrospiro[indene-1,3'-pyrrolidin]-5'-one (6S). A solution of **8a** (396 mg, 0.946 mmol) in absolute EtOH (52 mL) was hydrogenated at 90 °C and 90 bar of H$_2$ pressure in three passes over a Raney Ni cartridge using a ThalesNano H-cube hydrogenation reactor (flow rate 0.7 mL/min). The mixture was then evaporated; the residue was reconstituted in *p*-xylene (40 mL) and

heated in an oil bath thermostated at 155 °C. After 18 h the solvent was removed in vacuo and the residue subjected to flash column chromatography (EtOAc) followed by crystallization (EtOAc—hexane) to afford **6S** (215 mg, 75%) as a white powder: δ_H (400 MHz, CDCl$_3$) 1.53−1.63 (2H, m), 1.63−1.77 (2H, m), 1.79−1.88 (4H, m), 2.13 (1H, dt, J 12.7 and 7.5), 2.23 (1H, ddd, J 12.8, 7.0, and 6.2), 2.44 (1H, d, J 16.8), 2.61 (1H, d, J 16.8), 2.84−2.96 (2H, m), 3.42 (1H, d, J 9.5), 3.47 (1H, d, J 9.5), 3.81 (3H, s), 4.81−4.87 (1H, m), 6.55 (1H, br s), 6.77 (1H, d, J 8.2), 6.89 (1H, d, J 8.2); $[\alpha]_D^{22}$ +11.1 (c 1.08, CHCl$_3$). Anal. (C$_{18}$H$_{23}$NO$_3$) C, H, N.

(*R*)-4-Cyclopentyloxy-5-methoxy-2,3-dihydrospiro[indene-1,3′-pyrrolidin]-5′-one (6R). Following the procedure for **6S**, enantiomer **6R** (106 mg) was prepared in 38% yield from **8b** (383 mg): $[\alpha]_D^{22}$ −12.1 (c 1.09, CHCl$_3$). Anal. (C$_{18}$H$_{23}$NO$_3$) C, H, N.

(*R*)-4-(3-Cyclopentyloxy-4-methoxyphenyl)-1-methylpyrrolidin-2-one (10R). To a stirred solution of (*R*)-(−)-rolipram (30.0 mg, 0.109 mmol) in anhydrous DMF (3 mL) at ambient temperature was added NaH (60% w/w dispersion in mineral oil; 6.0 mg, 0.15 mmol) followed after 10 min by MeI (0.014 mL, 0.22 mmol). After 16 h the mixture was diluted with EtOAc (50 mL), washed with brine (3 × 10 mL), dried (Na$_2$SO$_4$), and evaporated to afford a residue from which **10R** (27 mg, 86%) was isolated as a colorless oil by flash column chromatography (1:99 to 1:49 MeOH—CH$_2$Cl$_2$ gradient): δ_H (400 MHz, CDCl$_3$) 1.56−1.66 (2H, m), 1.78−1.97 (6H, m), 2.51 (1H, dd, J 16.8 and 8.4), 2.78 (1H, dd, J 16.8 and 9.1), 2.90 (3H, s), 3.36 (1H, dd, J 9.6 and 7.1), 3.48 (1H, app quintet, J 8.2), 3.71 (1H, dd, J 9.6 and 8.3), 3.83 (3H, s), 4.74−4.78 (1H, m), 6.73 (1H, d, J 2.2), 6.74 (1H, dd, J 8.0 and 2.2), 6.82 (1H, d, J 8.0); m/z (EI) 289 (M$^+$, 45%), 221 (89), 150 (100). HRMS (EI) calcd for M$^+$ C$_{17}$H$_{23}$NO$_3$ 289.1678, found 289.1665. Anal. (C$_{17}$H$_{23}$NO$_3$) C, H, N.

(*S*)-4-(3-Cyclopentyloxy-4-methoxyphenyl)-1-methylpyrrolidin-2-one (10S). Following the above procedure for **10R**, enantiomer **10S** (20 mg, 63%) was prepared from (*S*)-(+)-rolipram (30 mg, 0.11 mmol). Anal. (C$_{17}$H$_{23}$NO$_3$) C, H, N.

(*R*)-1-Benzyl-4-(3-cyclopentyloxy-4-methoxyphenyl)pyrrolidin-2-one (11R). To a stirred solution of (*R*)-(−)-rolipram (23.2 mg, 0.0845 mmol) in anhydrous DMF (5 mL) at ambient temperature was added NaH (60% w/w dispersion in mineral oil; 3.7 mg, 0.093 mmol) followed after 45 min by BnBr (0.011 mL, 0.093 mmol). After 20 h the mixture was diluted with Et$_2$O (75 mL), washed with brine (3 × 15 mL), dried (Na$_2$SO$_4$), and evaporated to afford a residue from which **11R** (23.4 mg, 76%) was isolated as a colorless oil by flash column chromatography (1:9 Et$_2$O—CH$_2$Cl$_2$): δ_H (400 MHz, CDCl$_3$) 1.55−1.65 (2H, m), 1.76−1.92 (6H, m), 2.58 (1H, dd, J 16.9 and 8.2), 2.86 (1H, dd, J 16.8 and 9.2), 3.24 (1H, dd, J 9.6 and 7.0), 3.47 (1H, app quintet, J 8.4), 3.61 (1H, dd, J 9.6 and 8.3), 3.81 (3H, s), 4.46 (1H, d, J 14.6), 4.55 (1H, d, J 14.6), 4.67−4.71 (1H, m), 6.66 (1H, d, J 2.1), 6.68 (1H, dd, J 8.2 and 2.1), 6.77 (1H, d, J 8.2), 7.25−7.25 (5H, m). Anal. (C$_{23}$H$_{27}$NO$_3$) C, H, N.

(*S*)-1-Benzyl-4-(3-cyclopentyloxy-4-methoxyphenyl)pyrrolidin-2-one (11S). Following the above procedure for **11R**, enantiomer **11S** (25 mg, 94%) was prepared in an identical manner from (*S*)-rolipram (20 mg, 0.073 mmol). Anal. (C$_{23}$H$_{27}$NO$_3$) C, H, N.

Methyl 3-(3-Benzyloxy-4-methoxyphenyl)-4-nitrobutanoate (14). A stirred suspension of (methoxycarbonylmethylene)triphenylphosphorane (152 g, 456 mmol) and 3-benzyloxy-4-methoxybenzaldehyde (102 g, 419 mmol) was refluxed in MeCN (600 mL). After 7 h the dark brown homogeneous solution was cooled and evaporated to dryness. The solid residue comprising alkene **13** and Ph$_3$PO was resuspended in MeNO$_2$ (500 mL). 1,1,3,3-Tetramethylguanidine (12 mL) was added and the stirred mixture heated at 75 °C for 24 h. The mixture was then cooled and concentrated in vacuo. Ph$_3$PO was partially removed by crystallization of the residual oil from Et$_2$O (600 mL) and filtration. The filtrate was evaporated and subjected to flash column chromatography (1:9 to 1:4 EtOAc—light petroleum gradient to afford **14** (105 g, 70%) as a colorless

solid: δ_H (400 MHz, CDCl$_3$) 2.66 (1H, dd, J 13.9 and 5.3), 2.71 (1H, dd, J 13.9 and 5.0), 3.60 (3H, s), 3.83−3.90 (1H, m), 3.85 (3H, s), 4.52 (1H, dd, J 12.5 and 7.8), 4.64 (1H, dd, J 12.5 and 7.1), 5.12 (2H, s), 6.74 (1H, d, J 2.1), 6.77 (1H, dd, J 8.3 and 2.1), 6.84 (1H, d, J 8.2), 7.29−7.33 (1H, m), 7.35−7.39 (2H, m), 7.41−7.44 (2H, m); m/z (EI) 359 (M$^+$, 11%), 91 (100). Anal. (C$_{19}$H$_{21}$NO$_6$) C, H, N.

3-(3-Benzyloxy-4-methoxyphenyl)-4-nitrobutanoic Acid (15). To a stirred solution of **14** (6.50 g, 18.1 mmol) in MeOH (120 mL) at 0 °C was added dropwise NaOH solution (2 M, 60 mL). The mixture was allowed to attain ambient temperature over 16 h and then concentrated in vacuo. The residual oil was partitioned between hydrochloric acid (2 M, 60 mL) and EtOAc (150 mL), separating and further extracting the aqueous layer with EtOAc (2 × 40 mL). The combined organic phase was washed with brine (50 mL), dried (MgSO$_4$), and evaporated to afford **15** (5.89 g, 94%) as a beige powder: δ_H (400 MHz, CDCl$_3$) 2.69 (1H, dd, J 15.2 and 6.2), 2.75 (1H, dd, J 15.2 and 5.7), 3.80−3.88 (1H, m), 3.85 (3H, s), 4.50 (1H, dd, J 12.5 and 7.7), 4.61 (1H, dd, J 12.5 and 7.1), 5.11 (2H, s), 6.73 (1H, d, J 2.1), 6.77 (1H, dd, J 8.3 and 2.1), 6.84 (1H, d, J 8.3), 7.28−7.33 (1H, m), 7.34−7.39 (2H, m), 7.40−7.43 (2H, m), 9.93 (1H, br s); m/z (EI) 345 (M$^+$, 74%), 91 (100). Anal. (C$_{18}$H$_{19}$NO$_6$) C, H, N.

3-(3-(Benzyloxy)-4-methoxyphenyl)-4-nitrobutanoyl Chloride (16). A solution of **15** (5.85 g, 16.9 mmol) in anhydrous CH$_2$Cl$_2$ (55 mL) was refluxed with SOCl$_2$ (2.04 mL, 28.0 mmol). After 16 h the volatiles were removed in vacuo to afford **16** (6.13 g, 99%) as an amorphous yellow solid: δ_H (400 MHz, CDCl$_3$) 3.24 (1H, dd, J 17.5 and 8.0), 3.31 (1H, dd, J 17.5 and 6.4), 3.84−3.93 (1H, m), 3.86 (3H, s), 4.51 (1H, dd, J 12.8 and 7.3), 4.56 (1H, dd, J 12.8 and 7.6), 5.13 (2H, s), 6.71 (1H, d, J 2.2), 6.77 (1H, dd, J 8.3 and 2.2), 6.86 (1H, d, J 8.3), 7.30−7.34 (1H, m), 7.36−7.40 (2H, m), 7.41−7.44 (2H, m); MS (EI) m/z 363 (^{35}Cl M$^+$, 72%) 91 (100). Anal. (C$_{18}$H$_{18}$NO$_5$Cl) C, H, N.

(*R*)-3-(3-Benzyloxy-4-methoxyphenyl)-4-nitro-*N*-[(*S*)-1-phenylethyl]butanamide (17a) and (*S*)-3-[(3-Benzyloxy-4-methoxyphenyl)-4-nitro-*N*-[(*S*)-1-phenylethyl]butanamide (17b). To a solution of 3-(3-benzyloxy-4-methoxyphenyl)-4-nitrobutanoyl chloride (6.11 g, 16.8 mmol) in CH$_2$Cl$_2$ (65 mL) under reflux was added dropwise a solution of (*S*)-(−)-1-phenylethylamine (4.2 mL, 33.4 mmol) in CH$_2$Cl$_2$ (6 mL). After 2 h the mixture was cooled and washed successively with 2 M hydrochloric acid (50 mL), saturated NaHCO$_3$ solution (50 mL), and brine (50 mL). The organic phase was dried (MgSO$_4$) and evaporated to afford a 1:1 mixture of amides **17a** and **17b** (7.19 g, 96%) as a buff powder. The amides were partially separated by flash column chromatography (1:4:5 CH$_2$Cl$_2$—EtOAc—hexane) to afford **17a** (1.72 g) and **17b** (2.84 g) as colorless powders. Amide **17a**: TLC R_f = 0.37 (1:4:5 CH$_2$Cl$_2$—EtOAc—hexane); δ_H (400 MHz, CDCl$_3$) 1.30 (3H, d, J 6.9), 2.41 (1H, dd, J 14.5 and 7.5), 2.52 (1H, dd, J 14.5 and 6.9), 3.81−3.88 (1H, m), 3.86 (3H, s), 4.56 (1H, dd, J 12.5 and 8.0), 4.70 (1H, dd, J 12.5 and 6.4), 4.99 (1H, quintet, J 7.2), 5.08 (1H, d, J 12.2), 5.11 (1H, d, J 12.2), 5.39 (1H, br d, J 7.9), 6.71 (1H, d, J 2.1), 6.74 (1H, dd, J 8.2 and 2.1), 6.80 (1H, d, J 8.1), 7.13−7.16 (2H, m), 7.22−7.35 (6H, m), 7.39−7.42 (2H, m); MS (EI) m/z 448 (M$^+$, 8%), 105 (100). HRMS (EI) calcd for M$^+$ C$_{26}$H$_{28}$N$_2$O$_5$ 448.1998, found 448.1993. Anal. (C$_{26}$H$_{28}$N$_2$O$_5$) C, H, N. Amide **17b**: TLC R_f = 0.24 (1:4:5 CH$_2$Cl$_2$—EtOAc—hexane); δ_H (400 MHz, CDCl$_3$) 1.38 (3H, d, J 6.9), 2.34 (1H, dd, J 14.2 and 8.3), 2.55 (1H, dd, J 14.2 and 6.4), 3.83−3.90 (1H, m), 3.87 (3H, s), 4.58 (1H, dd, J 12.4 and 8.1), 4.67 (1H, dd, J 12.4 and 6.6), 4.99 (1H, quintet, J 7.3), 5.06 (1H, d, J 12.3), 5.09 (1H, d, J 12.3), 5.33 (1H, br d, J 7.9), 6.69 (1H, d, J 2.1), 6.73 (1H, dd, J 8.3 and 2.1), 6.79 (1H, d, J 8.3), 6.93−6.96 (2H, m), 7.18−7.34 (6H, m), 7.36−7.39 (2H, m); MS (EI) m/z 448 (M$^+$, 13%), 105 (100). HRMS (EI) calcd for M$^+$ C$_{26}$H$_{28}$N$_2$O$_5$ 448.1998, found 448.1997. Anal. (C$_{26}$H$_{28}$N$_2$O$_5$) C, H, N.

(*S*)-4-(3-Hydroxy-4-methoxyphenyl)pyrrolidin-2-one (18S). Amide **17b** (2.65 g, 5.91 mmol) was hydrogenated over 10% Pd/C as a solution in EtOAc and EtOH (1:1 v/v, 250 mL) using a ThalesNano

H-Cube (90 °C, 90 bar H_2, flow rate 0.8 mL/min). The crude aminoamide (1.76 g) obtained following evaporation of the eluate was reconstituted with p-xylene (150 mL) and heated in a sealed pressure vessel at 160 °C for 36 h to facilitate closure of the lactam ring. The solvent was then removed in vacuo and the resulting residue subjected to flash column chromatography (5:95 MeOH−EtOAc) to afford **18S** (990 mg, 81%) as a light brown powder: δ_H (400 MHz, CD_3OD−$CDCl_3$) 2.30 (1H, dd, J 17.0 and 8.7), 2.53 (1H, dd, J 17.0 and 8.9), 3.22 (1H, dd, J 9.7 and 7.3), 3.45 (1H, app. quintet, J 8.1), 3.58 (1H, dd, J 9.7 and 8.2), 3.71 (3H, s), 6.54 (1H, ddd, J 8.2, 2.2, and 0.5), 6.62 (1H, d, J 2.2), 6.67 (1H, d, J 8.3); MS m/z (EI) 207 (M^+, 90%), 150 (100), 135 (64). Anal. ($C_{11}H_{13}NO_3$) C, H, N.

(R)-4-(3-Hydroxy-4-methoxyphenyl)pyrrolidin-2-one (18R). **18R** was prepared as described for **18S** in 43% yield from **17a** (1.92 g). Anal. ($C_{11}H_{13}NO_3$) C, H, N.

(R)-4-(3,4-Dimethoxyphenyl)pyrrolidin-2-one (19R). To a stirred mixture of **18R** (115 mg, 0.555 mmol) and finely powdered K_2CO_3 (460 mg, 3.33 mmol) in anhydrous DMF (58 mL) was added iodomethane (70 μL, 1.1 mmol). After 42 h the mixture was filtered over Celite and the filtrate concentrated in vacuo. The resulting residue was subjected to flash column chromatography (2:98 MeOH−EtOAc) to afford **19R** (107 mg, 87%) as a pale yellow powder: δ_H (400 MHz, $CDCl_3$) 2.48 (1H, dd, J 16.9 and 8.8), 2.72 (1H, dd, J 16.9 and 8.9), 3.40 (1H, dd, J 9.2 and 7.3), 3.65 (1H, app quintet, J 8.2), 3.74−3.79 (1H, m), 3.87 (3H, s), 3.89 (3H, s), 5.86 (1H, br s), 6.75 (1H, d, J 2.0), 6.80 (1H, dd, J 8.2 and 2.0), 6.84 (1H, J 8.2); m/z (EI) 221 (M^+, 64%), 164 (100). Anal. ($C_{12}H_{15}NO_3$) C, H, N.

(S)-4-(3,4-Dimethoxyphenyl)pyrrolidin-2-one (19S). 19S was prepared as described for **19R** in 97% yield from **18S** (120 mg). Anal. ($C_{12}H_{15}NO_3$) C, H, N.

(R)-4-(3-Ethoxy-4-methoxyphenyl)pyrrolidin-2-one (20R). **20R** was prepared as described for **19R** in 78% yield from **18R** (157 mg) and iodoethane: δ_H (400 MHz, $CDCl_3$) 1.45 (3H, t, J 7.0), 2.47 (1H, dd, J 16.9 and 8.9), 2.70 (1H, dd, J 16.9 and 8.9), 3.38 (1H, dd, J 9.4 and 7.4), 3.62 (1H, app quintet, J 8.2), 3.72−3.77 (1H, m), 3.85 (3H, s), 4.09 (2H, q, J 7.0), 6.54 (1H, br s), 6.75 (1H, d, J 2.0), 6.78 (1H, dd, J 8.2 and 2.0), 6.82 (1H, J 8.2); m/z (EI) 235 (M^+, 100%). Anal. ($C_{13}H_{17}NO_3$) C, H, N.

(S)-4-(3-Ethoxy-4-methoxyphenyl)pyrrolidin-2-one (20S). **20S** was prepared as described for **19R** in 96% yield from **18S** (302 mg) and iodoethane. Anal. ($C_{13}H_{17}NO_3$) C, H, N.

(R)-4-(4-Methoxy-3-propyloxyphenyl)pyrrolidin-2-one (21R). **21R** was prepared as described for **19R** in 95% yield from **18R** (400 mg) and 1-iodopropane: δ_H (400 MHz, $CDCl_3$) 1.04 (3H, t, J 7.4), 1.85 (2H, sextet, J 7.4), 2.47 (1H, dd, J 16.9 and 8.9), 2.70 (1H, dd, J 16.9 and 8.9), 3.38 (1H, dd, J 9.4 and 7.4), 3.62 (1H, app quintet, J 8.4), 3.72−3.77 (1H, m), 3.84 (3H, s), 3.96 (2H, t, J 6.8), 6.59 (1H, br s), 6.75−6.79 (2H, m), 6.82 (1H, J 8.1); m/z (EI) 249 (M^+, 59%), 150 (100). Anal. ($C_{14}H_{19}NO_3$) C, H, N.

(S)-4-(4-Methoxy-3-propyloxyphenyl)pyrrolidin-2-one (21S). **21S** was prepared as described for **19R** in 95% yield from **18S** (120 mg) and 1-iodopropane. Anal. ($C_{14}H_{19}NO_3$) C, H, N.

8-[(Trimethylsilyl)ethynyl]-1,7-naphthyridin-6-amine (23). A sealable 500 mL pressure vessel was charged with **22**[36] (2.24 g, 8.50 mmol, prepared as described in the Supporting Information) and a mixture of THF and Et_3N (4:1 v/v, 250 mL) under Ar. To the resulting turbid mixture was added $(Ph_3P)_2PdCl_2$ (580 mg, 0.826 mmol), CuI (290 mg, 1.52 mmol), and (trimethylsilyl)acetylene (7.00 mL, 49.9 mmol). The vessel was sealed and the mixture stirred for 1 h at 50 °C followed by 14 h at 70 °C. The vessel was then cooled and the mixture filtered through Celite, washing with EtOAc (150 mL). The filtrate was washed with water (250 mL) followed by brine (3 × 50 mL), dried (Na_2SO_4), and concentrated in vacuo. The title compound (617 mg, 30%) was isolated from the resulting residue as a light brown powder by flash column chromatography (1:3 to 1:1 EtOAc−light petroleum gradient): δ_H (200 MHz, $CDCl_3$) 0.32 (9H, s), 4.73 (2H, br s), 6.64 (1H, s), 7.33 (1H, dd, J 3.9 and 8.5), 7.79 (1H, dd, J 1.5 and 8.5), 8.71 (1H, dd, J 1.5 and 3.9).

8-Ethynyl-1,7-naphthyridin-6-amine (24). A solution of **23** (593 mg, 2.46 mmol) in THF (25 mL) was treated with tetrabutylammonium fluoride (1 M in 5% H_2O−THF solution; 2.71 mL, 2.71 mmol). After 10 min the mixture was concentrated in vacuo. The resulting residue was taken up in EtOAc (150 mL) and washed with water (3 × 25 mL). The organic phase was dried (Na_2SO_4) and concentrated in vacuo to afford a residue from which **24** (356 mg, 86%) was isolated as a yellow solid by flash column chromatography (1:19 MeOH−CH_2Cl_2): δ_H (200 MHz, $CDCl_3$) 3.62 (1H, s), 4.69 (2H, br s), 6.67 (1H, s), 7.36 (1H, dd, J 4.0 and 8.5), 7.83 (1H, dd, J 1.6 and 8.5), 8.75 (1H, dd, J 1.6 and 4.0).

8-Ethyl-1,7-naphthyridin-6-amine (25). A solution of **24** (350 mg, 2.07 mmol) in EtOH (30 mL) was hydrogenated at 1 atm over 10% Pd−C (121 mg) at ambient temperature for 10 h. The reaction mixture was then purged with N_2 and filtered over Celite, washing with $CHCl_3$. The filtrate was evaporated to afford a residue from which **25** (263 mg, 73%) was isolated by flash column chromatography (2.5:97.5 MeOH−CH_2Cl_2): δ_H (200 MHz, $CDCl_3$) 1.36 (3H, t, J 7.5), 3.36 (2H, q, J 7.5), 4.57 (2H, s), 6.46 (1H, s), 7.29 (1H, dd, J 4.1 and 8.4), 7.75 (1H, dd, J 1.7 and 8.5), 8.61 (1H, dd, J 1.7 and 4.1); m/z (EI) 173 (M^+, 38%), 172 (M^+ − H, 100). HRMS (ESI+) calcd for MH^+ $C_{10}H_{12}N_3$ 174.1026, found 174.1027.

8-Ethyl-1,7-naphthyridin-6-yl Trifluoromethanesulfonate (26). To an ice-cooled solution of **25** (256 mg, 1.48 mmol) in DMF (4 mL) was added trifluoromethanesulfonic acid (1.0 mL, 11.3 mmol) followed after 5 min by $NaNO_2$ (204 mg, 2.96 mmol) in small portions. After the addition the mixture was stirred at 0 °C for 2 h and then at ambient temperature for a further 2 h. The mixture was then diluted with EtOAc (80 mL) and washed successively with water (20 mL), 2 M NaOH solution (10 mL), and water (2 × 10 mL). The organic phase was dried (Na_2SO_4) and concentrated in vacuo to afford **26** (239 mg, 53%) as an orange oil: δ_H (200 MHz, $CDCl_3$) 1.38 (3H, t, J 7.5), 3.49 (2H, q, J 7.5), 7.36 (1H, s), 7.60 (1H, dd, J 4.1 and 8.5), 8.14 (1H, dd, J 1.7 and 8.5), 8.99 (1H, dd, J 1.7 and 4.1).

Methyl 4-(8-Ethyl-1,7-naphthyridin-6-yl)benzoate (27). A stirred solution of **26** (239 mg, 0.780 mmol), 4-(methoxycarbonyl)phenylboronic acid (183 mg, 1.02 mmol), Ph_3P (16 mg, 0.061 mmol), and bis(dibenzylideneacetone)palladium(0) (18 mg, 0.031 mmol) in THF (6 mL) was heated with 2 M Na_2CO_3 solution (1.5 mL) in a bath thermostated at 80 °C. After 17 h the brown mixture was cooled, diluted with EtOAc (50 mL), filtered through Celite, and washed with brine (3 × 10 mL). The organic phase was dried (Na_2SO_4) and concentrated in vacuo to give a residue from which **27** (175 mg, 77%) was isolated by flash column chromatography (1:4 EtOAc−light petroleum) as a colorless solid: δ_H (200 MHz, $CDCl_3$) 1.50 (3H, t, J 7.5), 3.58 (2H, q, J 7.5), 3.92 (3H, s), 7.54 (1H, dd, J 4.2 and 8.3), 7.91 (1H, s), 8.11−8.18 (3H, m), 8.25 (2H, m), 8.95 (1H, dd, J 1.7 and 4.2).

4-(8-Ethyl-1,7-naphthyridin-6-yl)benzoic Acid (28). A solution of LiOH·H_2O (50.2 mg, 1.20 mmol) in water (4 mL) was added to a stirred solution of **27** (175 mg, 0.599 mmol) in a mixture of THF and MeOH (2:1, 6 mL) at ambient temperature. After 20 h the mixture was concentrated in vacuo to remove the organic solvent and the aqueous residue adjusted to pH 6 by addition of 2 M HCl, depositing a fine white precipitate of product (42 mg) that was collected by filtration. The filtrate was extracted with EtOAc (50 mL) and the organic layer subsequently washed with brine (3 × 10 mL), dried (Na_2SO_4), and evaporated. A second batch of product (57 mg) was isolated from the residual pale yellow solid following trituration with Et_2O (15 mL) to afford **28** (99.0 mg in total, 59%) as a colorless powder: δ_H (200 MHz, DMSO-d_6) 1.40 (3H, t, J 7.5), 3.50 (2H, q, J 7.5), 7.78 (1H, dd, J 4.1 and 8.4), 8.08 (2H, m), 8.35 (2H, m), 8.42 (1H, s), 8.44 (1H, dd, J 1.7 and 8.4), 9.02 (1H, dd, J 1.7 and 4.1). HRMS (EI) calcd for M^+ $C_{17}H_{14}N_2O_2$ 279.1128, found 279.1128. Anal. ($C_{17}H_{14}N_2O_2$) C, H, N.

X-ray CIF Files. The X-ray CIF files for (*rac*)-**6** and **9** have been deposited at the Cambridge Crystallographic Data Center with the deposition numbers CCDC 808534 and CCDC 808535. Copies of the data can be obtained, free of charge, from CCDC, 12 Union Road, Cambridge, CB2 1EZ, U.K. (e-mail, deposit@ccdc.cam.ac.uk; Internet, http://www.ccdc.cam.ac.uk/).

■ ASSOCIATED CONTENT

ⓢ Supporting Information. Experimental procedures for preparation of **2** and **22**; procedures for the derivatization of **6S** and **18S** as **9** and (*S*)-rolipram, respectively; crystallographic data for (*rac*)-**6** and **9** (Figure S1); ^{1}H and ^{13}C NMR data presented with signal assignments; compound elemental analysis data; melting point and IR data; comparison of PDE4 binding modes for rolipram and NVP (Figure S2); CAS registry numbers, primary references, and structures for PDE4 inhibitors listed in Figure 2 (Figure S3). This material is available free of charge via the Internet at http://pubs.acs.org.

■ AUTHOR INFORMATION

Corresponding Author
*Phone: +44 (0)131 221 9790. Fax: +44 (0)131 221 3180. E-mail: D.R.Adams@hw.ac.uk.

■ ACKNOWLEDGMENT

■ ABBREVIATIONS USED

cAMP, cyclic adenosine 3′,5′-monophosphate; CHO, Chinese hamster ovary; COPD, chronic obstructive pulmonary disease; DISC1, disrupted-in-schizophrenia 1; GFP, green fluorescent protein; LR1, linker region 1; LR2, linker region 2; p62/SQSTM-1, sequestosome-1; mTor, mammalian target of rapamycin; p75^{NTR}, p75 neurotrophin receptor; PDE4, phosphodiesterase type 4; PKA, protein kinase A; TOSMIC, toluenesulfonylmethyl isocyanide; TNF, tumor necrosis factor; UCR1, upstream conserved region 1; UCR2, upstream conserved region 2; WT, wild type

■ REFERENCES

(1) Conti, M.; Richter, W.; Mehats, C.; Livera, G.; Park, J. Y.; Jin, C. Cyclic AMP-specific PDE4 phosphodiesterases as critical components of cyclic AMP signaling. *J. Biol. Chem.* **2003**, *278*, 5493–5496.

(2) Houslay, M. D.; Adams, D. R. PDE4 cAMP phosphodiesterases: modular enzymes that orchestrate signalling cross-talk, desensitization and compartmentalization. *Biochem. J.* **2003**, *370*, 1–18.

(3) Le Jeune, I. R.; Shepherd, M.; Van Heeke, G.; Houslay, M. D.; Hall, I. P. Cyclic AMP-dependent transcriptional up-regulation of phosphodiesterase 4D5 in human airway smooth muscle cells: identification and characterization of a novel PDE4D5 promoter. *J. Biol. Chem.* **2002**, *277*, 35980–35989.

(4) Monaco, L.; Vicini, E.; Conti, M. Structure of 2 rat genes coding for closely-related rolipram-sensitive cAMP phosphodiesterases: multiple messenger-RNA variants originate from alternative splicing and multiple start sites. *J. Biol. Chem.* **1994**, *269*, 347–357.

(5) Vicini, E.; Conti, M. Characterization of an intronic promoter of a cyclic adenosine 3′,5′-monophosphate (cAMP): specific phosphodiesterase gene that confers hormone and cAMP inducibility. *Mol. Endocrinol.* **1997**, *11*, 839–850.

(6) Wallace, D. A.; Johnston, L. A.; Huston, E.; MacMaster, D.; Houslay, T. M.; Cheung, Y. F.; Campbell, L.; Millen, J. E.; Smith, R. A.; Gall, I.; Knowles, R. G.; Sullivan, M.; Houslay, M. D. Identification and characterization of PDE4A11, a novel, widely expressed long isoform encoded by the human PDE4A cAMP phosphodiesterase gene. *Mol. Pharmacol.* **2005**, *67*, 1920–1934.

(7) Rena, G.; Begg, F.; Ross, A.; Mackenzie, C.; McPhee, I.; Campbell, L.; Huston, E.; Sullivan, M.; Houslay, M. D. Molecular cloning, genomic positioning, promoter identification, and characterization of the novel cyclic AMP-specific phosphodiesterase PDE4A10. *Mol. Pharmacol.* **2001**, *59*, 996–1011.

(8) Houslay, M. D.; Baillie, G. S.; Maurice, D. H. cAMP-specific phosphodiesterase-4 enzymes in the cardiovascular system: a molecular toolbox for generating compartmentalized cAMP signaling. *Circ. Res.* **2007**, *100*, 950–966.

(9) Baillie, G. S.; Scott, J. D.; Houslay, M. D. Compartmentalisation of phosphodiesterases and protein kinase A: opposites attract. *FEBS Lett.* **2005**, *579*, 3264–3270.

(10) Baillie, G. S.; Houslay, M. D. Arrestin times for compartmentalised cAMP signalling and phosphodiesterase-4 enzymes. *Curr. Opin. Cell Biol.* **2005**, *17*, 129–134.

(11) Houslay, M. D. Underpinning compartmentalised cAMP signalling through targeted cAMP breakdown. *Trends Biochem. Sci.* **2010**, *35*, 91–100.

(12) McCahill, A. C.; Huston, E.; Li, X.; Houslay, M. D. PDE4 associates with different scaffolding proteins: modulating interactions as treatment for certain diseases. *Handb. Exp. Pharmacol.* **2008**, 125–166.

(13) Sachs, B. D.; Akassoglou, K. Regulation of cAMP by the p75 neurotrophin receptor: insight into drug design of selective phosphodiesterase inhibitors. *Biochem. Soc. Trans.* **2007**, *35*, 1273–1277.

(14) Sachs, B. D.; Baillie, G. S.; McCall, J. R.; Passino, M. A.; Schachtrup, C.; Wallace, D. A.; Dunlop, A. J.; MacKenzie, K. F.; Klussmann, E.; Lynch, M. J.; Sikorski, S. L.; Nuriel, T.; Tsigelny, I.; Zhang, J.; Houslay, M. D.; Chao, M. V.; Akassoglou, K. p75 neurotrophin receptor regulates tissue fibrosis through inhibition of plasminogen activation via a PDE4/cAMP/PKA pathway. *J. Cell Biol.* **2007**, *177*, 1119–1132.

(15) Barber, R.; Baillie, G. S.; Bergmann, R.; Shepherd, M. C.; Sepper, R.; Houslay, M. D.; Heeke, G. V. Differential expression of PDE4 cAMP phosphodiesterase isoforms in inflammatory cells of smokers with COPD, smokers without COPD, and nonsmokers. *Am. J. Physiol.: Lung Cell. Mol. Physiol.* **2004**, *287*, L332–L343.

(16) Hannila, S. S.; Filbin, M. T. The role of cyclic AMP signaling in promoting axonal regeneration after spinal cord injury. *Exp. Neurol.* **2008**, *209*, 321–332.

(17) Sharafkhaneh, A.; Jayaraman, G.; Kaleekal, T.; Sharafkhaneh, H.; Hirshkowitz, M. Sleep disorders and their management in patients with COPD. *Ther. Adv. Respir. Dis.* **2009**, *3*, 309–318.

(18) Vecsey, C. G.; Baillie, G. S.; Jaganath, D.; Havekes, R.; Daniels, A.; Wimmer, M.; Huang, T.; Brown, K. M.; Li, X. Y.; Descalzi, G.; Kim, S. S.; Chen, T.; Shang, Y. Z.; Zhuo, M.; Houslay, M. D.; Abel, T. Sleep deprivation impairs cAMP signalling in the hippocampus. *Nature* **2009**, *461*, 1122–1125.

(19) Terry, R.; Cheung, Y. F.; Praestegaard, M.; Baillie, G. S.; Huston, E.; Gall, I.; Adams, D. R.; Houslay, M. D. Occupancy of the catalytic site of the PDE4A4 cyclic AMP phosphodiesterase by rolipram triggers the dynamic redistribution of this specific isoform in living cells through a cyclic AMP independent process. *Cell. Signalling* **2003**, *15*, 955–971.

(20) Christian, F.; Anthony, D. F.; Vadrevu, S.; Riddell, T.; Day, J. P.; McLeod, R.; Adams, D. R.; Baillie, G. S.; Houslay, M. D. p62 (SQSTM1) and cyclic AMP phosphodiesterase-4A4 (PDE4A4) locate to a novel, reversible protein aggregate with links to autophagy and proteasome degradation pathways. *Cell. Signalling* **2010**, *22*, 1576–1596.

(21) Pankiv, S.; Lamark, T.; Bruun, J. A.; Overvatn, A.; Bjorkoy, G.; Johansen, T. Nucleocytoplasmic shuttling of p62/SQSTM1 and its role in recruitment of nuclear polyubiquitinated proteins to promyelocytic leukemia bodies. *J. Biol. Chem.* **2010**, *285*, 5941–5953.

(22) Moscat, J.; Diaz-Meco, M. T. p62 at the crossroads of autophagy, apoptosis, and cancer. *Cell* **2009**, *137*, 1001–1004.

(23) Ichimura, Y.; Komatsu, M. Selective degradation of p62 by autophagy. *Semin. Immunopathol.* **2010**, *32*, 431–436.

(24) Kim, H. W.; Ha, S. H.; Lee, M. N.; Huston, E.; Kim, D. H.; Jang, S. K.; Suh, P. G.; Houslay, M. D.; Ryu, S. H. Cyclic AMP controls mTOR through regulation of the dynamic interaction between Rheb and phosphodiesterase 4D. *Mol. Cell. Biol.* **2010**, *30*, 5406–5420.

(25) Card, G. L.; England, B. P.; Suzuki, Y.; Fong, D.; Powell, B.; Lee, B.; Luu, C.; Tabrizizad, M.; Gillette, S.; Ibrahim, P. N.; Artis, D. R.; Bollag, G.; Milburn, M. V.; Kim, S. H.; Schlessinger, J.; Zhang, K. Y. J. Structural basis for the activity of drugs that inhibit phosphodiesterases. *Structure* **2004**, *12*, 2233–2247.

(26) Huai, Q.; Wang, H. C.; Sun, Y. J.; Kim, H. Y.; Liu, Y. D.; Ke, H. M. Three-dimensional structures of PDE4D in complex with roliprams and implication on inhibitor selectivity. *Structure* **2003**, *11*, 865–873.

(27) Xu, R. X.; Rocque, W. J.; Lambert, M. H.; Vanderwall, D. E.; Luther, M. A.; Nolte, R. T. Crystal structures of the catalytic domain of phosphodiesterase 4B complexed with AMP, 8-Br-AMP, and rolipram. *J. Mol. Biol.* **2004**, *337*, 355–365.

(28) Zhang, K. Y. J.; Card, G. L.; Suzuki, Y.; Artis, D. R.; Fong, D.; Gillette, S.; Hsieh, D.; Neiman, J.; West, B. L.; Zhang, C.; Milburn, M. V.; Kim, S. H.; Schlessinger, J.; Bollag, G. A glutamine switch mechanism for nucleotide selectivity by phosphodiesterases. *Mol. Cell* **2004**, *15*, 279–286.

(29) A variety of metal ions may occupy the Me2 site and support catalytic activity, but the physiologically relevant ion, which also occupies the site in the majority of PDE4 crystal structures, is Mg^{2+}. In the 1RO6 structure the Me2 site is occupied by Mn^{2+} (or a mixed Mn^{2+}/Ca^{2+} population). We considered that the presence of the Mn^{2+} ion, with a slightly larger ionic radius than Mg^{2+}, might simulate the enzyme with its catalytic pocket in a mildly contracted state.

(30) Kemperman, G. J.; Roeters, T. A.; Hilberink, P. W. Cleavage of aromatic methyl ethers by chloroaluminate ionic liquid reagents. *Eur. J. Org. Chem.* **2003**, 1681–1686.

(31) Keller, T. H.; Bray-French, K.; Demnitz, F. W.; Muller, T.; Pombo-Villar, E.; Walker, C. Synthesis and structure–activity relationship of N-arylrolipram derivatives as inhibitors of PDE4 isozymes. *Chem. Pharm. Bull. (Tokyo)* **2001**, *49*, 1009–1017.

(32) Bolger, G. B.; Baillie, G. S.; Li, X.; Lynch, M. J.; Herzyk, P.; Mohamed, A.; Mitchell, L. H.; McCahill, A.; Hundsrucker, C.; Klussmann, E.; Adams, D. R.; Houslay, M. D. Scanning peptide array analyses identify overlapping binding sites for the signalling scaffold proteins, β-arrestin and RACK1, in cAMP-specific phosphodiesterase PDE4D5. *Biochem. J.* **2006**, *398*, 23–36.

(33) We also initially considered an alternative model in which the N-alkyl groups in **10S** and **11S** might ablate the foci-forming property of (S)-rolipram by obstructing an induced fit of the inhibitor within the Q_2 subpocket rather than obstructing protein docking or folding. Such a fit could conceivably drive structural transition leading to foci formation by exerting leverage at the junction between helices 14 and 15. Occupancy of the Q_2 pocket in PDE5, typically with more penetrating hydrophobic substituents, is important for achieving high affinity binding of inhibitors.[51,52] Such occupancy undoubtedly influences the conformation of the enzyme's M-loop, encompassing the connecting sequence between helices 14 and 15, albeit that the situation is likely complicated by coordinated movement in both H- and M-loops.[52,53] There is no evidence that the cognate regions in PDE4 share the extensive conformational and positional mobility of the PDE5 H- and M-loops. Nevertheless, the influential role of Q_2 occupancy in PDE5 suggested that this should be considered as a possible driver for structural transition in PDE4 and reinforced the decision to probe the role of the cyclopentyloxy group. Although the available cocrystal structures of rolipram (foci-inducer) and piclamilast and cilomilast (foci-blockers that share rolipram's 3-cyclopentyloxy-4-methoxyphenyl core) show no significant differences in the conformation of the M-loop, the induced fit model for PDE4A4 foci formation also required initial consideration because structural differences between the complexes of foci-blocker and foci-former might only be evident with the full-length enzyme; all of the currently available crystal structures are N-terminally truncated.

(34) Demnitz, J.; LaVecchia, L.; Bacher, E.; Keller, T. H.; Muller, T.; Schurch, F.; Weber, H. P.; Pombo-Villar, E. Enantiodivergent synthesis of (R)- and (S)-rolipram. *Molecules* **1998**, *3*, 107–119.

(35) Wang, H.; Peng, M. S.; Chen, Y.; Geng, J.; Robinson, H.; Houslay, M. D.; Cai, J.; Ke, H. Structures of the four subfamilies of phosphodiesterase-4 provide insight into the selectivity of their inhibitors. *Biochem. J.* **2007**, *408*, 193–201.

(36) Hersperger, R.; Bray-French, K.; Mazzoni, L.; Muller, T. Palladium-catalyzed cross-coupling reactions for the synthesis of 6,8-disubstituted 1,7-naphthyridines: a novel class of potent and selective phosphodiesterase type 4D inhibitors. *J. Med. Chem.* **2000**, *43*, 675–682.

(37) Huai, Q.; Liu, Y.; Francis, S. H.; Corbin, J. D.; Ke, H. Crystal structures of phosphodiesterases 4 and 5 in complex with inhibitor 3-isobutyl-1-methylxanthine suggest a conformation determinant of inhibitor selectivity. *J. Biol. Chem.* **2004**, *279*, 13095–13101.

(38) Burgin, A. B.; Magnusson, O. T.; Singh, J.; Witte, P.; Staker, B. L.; Bjornsson, J. M.; Thorsteinsdottir, M.; Hrafnsdottir, S.; Hagen, T.; Kiselyov, A. S.; Stewart, L. J.; Gurney, M. E. Design of phosphodiesterase 4D (PDE4D) allosteric modulators for enhancing cognition with improved safety. *Nat. Biotechnol.* **2010**, *28*, 63–70.

(39) Houslay, M. D.; Adams, D. R. Putting the lid on phosphodiesterase 4. *Nat. Biotechnol.* **2010**, *28*, 38–40.

(40) Lee, M. E.; Markowitz, J.; Lee, J. O.; Lee, H. Crystal structure of phosphodiesterase 4D and inhibitor complex(1). *FEBS Lett.* **2002**, *530*, 53–58.

(41) The amide carbonyl group of PDE4-bound piclamilast is orientated toward the position that would be occupied by Tyr286 in the UCR2-capped state but would not form a close contact (O···O distance of ~3.7 Å expected).

(42) Gibson, L. C.; Hastings, S. F.; McPhee, I.; Clayton, R. A.; Darroch, C. E.; Mackenzie, A.; Mackenzie, F. L.; Nagasawa, M.; Stevens, P. A.; Mackenzie, S. J. The inhibitory profile of ibudilast against the human phosphodiesterase enzyme family. *Eur. J. Pharmacol.* **2006**, *538*, 39–42.

(43) Johnston, K. A.; Allcock, R. W.; Jiang, Z.; Collier, I. D.; Blakli, H.; Rosair, G. M.; Bailey, P. D.; Morgan, K. M.; Kohno, Y.; Adams, D. R. Concise routes to pyrazolo[1,5-a]pyridin-3-yl pyridazin-3-ones. *Org. Biomol. Chem.* **2008**, *6*, 175–186.

(44) Alvarez, R.; Sette, C.; Yang, D.; Eglen, R. M.; Wilhelm, R.; Shelton, E. R.; Conti, M. Activation and selective inhibition of a cyclic AMP-specific phosphodiesterase, PDE-4D3. *Mol. Pharmacol.* **1995**, *48*, 616–622.

(45) McPhee, I.; Yarwood, S. J.; Scotland, G.; Huston, E.; Beard, M. B.; Ross, A. H.; Houslay, E. S.; Houslay, M. D. Association with the SRC family tyrosyl kinase LYN triggers a conformational change in the catalytic region of human cAMP-specific phosphodiesterase HSPDE4A4B. Consequences for rolipram inhibition. *J. Biol. Chem.* **1999**, *274*, 11796–11810.

(46) Saldou, N.; Obernolte, R.; Huber, A.; Baecker, P. A.; Wilhelm, R.; Alvarez, R.; Li, B.; Xia, L.; Callan, O.; Su, C.; Jarnagin, K.; Shelton, E. R. Comparison of recombinant human PDE4 isoforms: interaction with substrate and inhibitors. *Cell. Signalling* **1998**, *10*, 427–440.

(47) Houslay, M. D.; Christian, F. p62 (SQSTM1) forms part of a novel, reversible aggregate containing a specific conformer of the cAMP degrading phosphodiesterase, PDE4A4. *Autophagy* **2010**, *6*, 1198–1200.

(48) Huston, E.; Pooley, L.; Julien, P.; Scotland, G.; McPhee, I.; Sullivan, M.; Bolger, G.; Houslay, M. D. The human cyclic AMP-specific phosphodiesterase PDE-46 (HSPDE4A4B) expressed in transfected COS7 cells occurs as both particulate and cytosolic species that exhibit distinct kinetics of inhibition by the antidepressant rolipram. *J. Biol. Chem.* **1996**, *271*, 31334–31344.

(49) Lobban, M.; Shakur, Y.; Beattie, J.; Houslay, M. D. Identification of two splice variant forms of type-IVB cyclic AMP phosphodiesterase, DPD (rPDE-IVB1) and PDE-4 (rPDE-IVB2) in brain: selective localization in membrane and cytosolic compartments and differential expression in various brain regions. *Biochem. J.* **1994**, *304*, 399–406.

(50) Gottlieb, H. E.; Kotlyar, V.; Nudelman, A. NMR chemical shifts of common laboratory solvents as trace impurities. *J. Org. Chem.* **1997**, *62*, 7512–7515.

(51) Allerton, C. M.; Barber, C. G.; Beaumont, K. C.; Brown, D. G.; Cole, S. M.; Ellis, D.; Lane, C. A.; Maw, G. N.; Mount, N. M.; Rawson, D. J.; Robinson, C. M.; Street, S. D.; Summerhill, N. W. A novel series of potent and selective PDE5 inhibitors with potential for high and dose-independent oral bioavailability. *J. Med. Chem.* **2006**, *49*, 3581–3594.

(52) Chen, G.; Wang, H.; Robinson, H.; Cai, J.; Wan, Y.; Ke, H. An insight into the pharmacophores of phosphodiesterase-5 inhibitors from synthetic and crystal structural studies. *Biochem. Pharmacol.* **2008**, *75*, 1717–1728.

(53) Wang, H.; Ye, M.; Robinson, H.; Francis, S. H.; Ke, H. Conformational variations of both phosphodiesterase-5 and inhibitors provide the structural basis for the physiological effects of vardenafil and sildenafil. *Mol. Pharmacol.* **2008**, *73*, 104–110.